

# DIFFERENT TECTONO-THERMAL EVOLUTIONARY PATHS IN ECLOGITIC ROCKS FROM THE AXIAL ZONE OF THE VARISCAN CHAIN IN SARDINIA (ITALY) COMPARED WITH THE LIGURIAN ALPS

**Luciano Cortesogno\***, **Laura Gaggero\***, **Giacomo Oggiano\*\*** and **Jean-Louis Paquette\*\*\***

\* Dipartimento per lo Studio del Territorio e delle sue Risorse, Università di Genova, Italy  
(e-mail: cortez@dipteris.unige.it).

\*\* Istituto di Scienze Geologico-Mineralogiche, Università di Sassari, Italy (e-mail: giacoggi@unissmain.it).

\*\*\* UMR6524 "Magmas et Volcans", Université B. Pascal, Clermont-Ferrand, France  
(e-mail: J.L.Paquette@opgc.univ-bpclermont.fr).

Corresponding Author: Laura Gaggero, e-mail gaggero@dipteris.unige.it

**Keywords:** Variscan orogen, meta-eclogite, granulite, U/Pb radiometric dating, Lower Palaeozoic, Ligurian Alps.

## ABSTRACT

The inner zone of the Sardinia Variscan segment consists of two metamorphic complexes:

I) A polymetamorphic Migmatite Complex, with migmatites showing polyphase anatetic processes, in the presence of kyanite or sillimanite. The Migmatite complex preserved decametric lenses of eclogite relicts (eclogites A) affected by high T, high- to intermediate P recrystallization under granulite facies conditions. The decompressional garnet + Ca-clinopyroxene + amphibole ± orthopyroxene-bearing assemblages developed in granoblastic textures generally in no stress conditions. In most cases, only symplectite textures provide evidence for the eclogitic event.

II) A medium grade, mostly metapelitic complex consisting of Grt, Ky, Stau-bearing micaschists and paragneisses includes quartzites and garnet-bearing amphibolite boudins with N-MORB chemical affinity. Relicts of eclogite assemblages were locally found in the metabasite (eclogites B).

In eclogites A, the geothermobarometric parameters yield temperatures in the range 690°–760°C for minimum pressure ≈1.3 GPa. Pyroxene compositions accord with temperatures in excess of 700°C. In eclogites B, the thermometric calibrations provide temperatures in the range 610°–700°C for pressures 1.3–1.5 GPa, based on the jadeite content. The temperatures are consistent with the biotite+muscovite+garnet+kyanite+staurolite assemblage in the host paragneisses, and with lack of anatetic processes.

The age of 457±2 Ma, obtained by U/Pb dating on one sample of Type A eclogite is interpreted as a minimum estimate for the magmatism of the eclogite protolith. A second zircon population defined an age of 403±4 Ma interpreted as dating the zircon crystallization during the high-grade event.

The relationships between Types A and B eclogites, and their bearing on the regional framework (Sardinia, Ligurian Alps) are discussed.

## INTRODUCTION

Within the Sardinia basement eclogites are known to occur within the Gallura High Grade Metamorphic Complex (Miller et al., 1976; Franceschelli et al., 1998) associated with migmatites affected by Late Variscan HT\LP metamorphic overprint. Eclogites are described also from within Grt, Ky, and Stau-bearing metapelites, close to an important retrograde transcurrent shear zone at regional scale. The micaschist belt hosting the eclogites was interpreted as a Variscan suture zone (Posada - Asinara line; Cappelli et al., 1992), as an accretionary mélange thrust on the northern Gondwana margin (Carmignani and Oggiano, 1997) or as a wide Variscan transpressional shear belt (Carosi and Palmeri, 2002). This article I) aims to compare the protolith nature and the PT conditions recorded during the metamorphic peak and the exhumation paths by the metabasites from the two complexes; II) tentatively approaches the regional implications by comparing the Sardinia metabasites with their homologous of the Ligurian Alps III) discusses their significance in the peri-Gondwanian framework, in the perspective of recent geodynamic reconstructions (Stampfli et al., 2002; von Raumer et al., 2003).

## GEOLOGICAL OUTLINE

The inner zone of the Sardinia Variscan chain (Fig. 1) is characterised by medium- to high-grade metamorphic rocks and consists of two metamorphic complexes (Fig. 1A):

I) A polymetamorphic Migmatite Complex (Figs. 1, 2) developed in the northernmost part of the island up to Corsica. The migmatites show polyphase anatetic processes, in the presence of kyanite or sillimanite.

In the Migmatite Complex, decametric basic lenses preserve eclogite relicts (eclogites A) affected by high T, high- to intermediate P recrystallization under granulite facies conditions (Miller et al., 1976; Ghezzo et al., 1979; 1982; Di Pisa et al., 1992; Franceschelli et al., 1998, 2002). The decompressional garnet+Ca-clinopyroxene+amphibole±orthopyroxene-bearing assemblages developed in granoblastic textures, generally under no stress conditions.

Paragenetic mineral relicts, of the pre-granulite history, other than zoning in garnet, are rarely preserved, so that in most cases only symplectite textures provide evidence for the eclogitic event.

II) A medium-grade, mostly metapelitic complex (Gneiss Complex; Figs. 1, 2A; 2B), consisting of Grt, Ky, Stau-bearing micaschists and paragneisses includes quartzites and garnet-bearing amphibolite boudins with N-MORB chemical affinity (Cappelli et al., 1992; Oggiano and Di Pisa, 1992). Relicts of eclogite assemblages were locally found in the metabasites (eclogites B).

The Gneiss Complex is confined along a narrow, NNW-trending belt (Posada-Asinara Line). Thrusting, or combined thrusting-wrenching, of the Migmatite Complex onto the Gneiss Complex (Fig. 2) is apparent in places where the contact is not complicated by late-Variscan retrograde strike-slip shears (Oggiano and Di Pisa 1992; Carosi and Oggiano, 2002). Within the collisional frame, the Migmatite

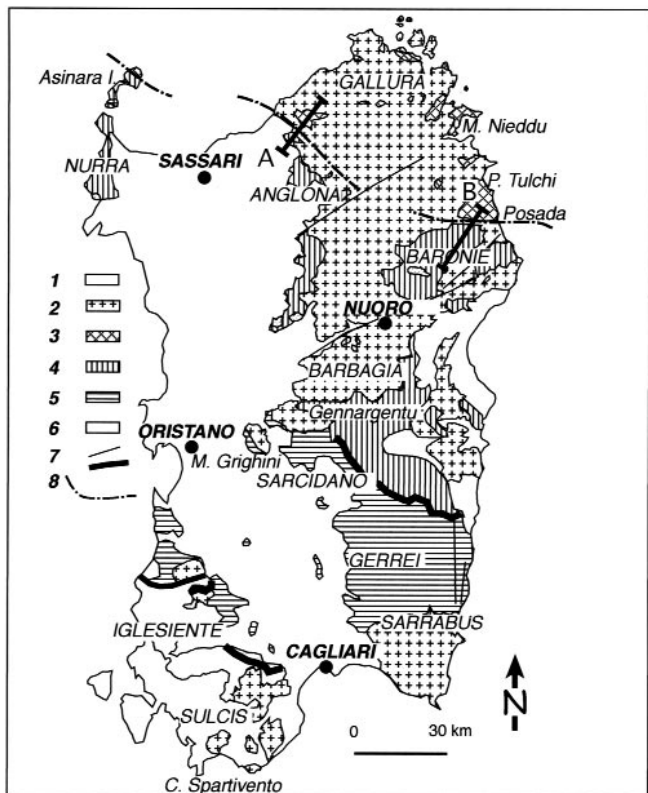


Fig. 1 - Main structural elements of the Sardinia basement: 1: Post - Variscan covers; 2: Late Hercynian batholith; 3: High grade metamorphic complex; 4: Internal nappes; 5: External nappes; 6: External zone; 7: Major and minor thrusts; 8: Posada - Asinara Line.

Complex has been regarded as a crustal nappe comparable to the inner crystalline nappe of the French Massif Central, whereas the high-strain Gneiss Complex has been regarded as the Sardinia segment of the south Variscan suture zone (Cappelli et al., 1992; Carmignani et al., 1994), re-equilibrated under intermediate-P amphibolite facies conditions.

Both complexes are overprinted by Late Variscan HT/LP re-equilibration, related to the late Carboniferous post-collisional gravitational collapse of the chain (Oggiano and Di Pisa, 1992; Di Pisa et al., 1992; Carmignani et al., 1994), mostly on the base of micas blocking ages and of meso- and micro-structural evidence (Del Moro et al., 1991).

## FIELD OCCURRENCE AND SAMPLING

The Migmatite Complex metabasites occur in the Costa Smeralda area as rotated boudins within andalusite+cordierite-bearing metatexites retaining relict mylonitic fabric. Elsewhere, metabasites are hosted within diatexitic rocks derived from both ortho- and paragneisses showing a sillimanite+K-feldspar assemblage. The structural relationships between metabasites and migmatites were obscured due to the strongly different rheology during the polyphase deformation.

Three samples preserving garnet-omphacite relicts were selected for detailed investigation from a decametric eclogite body hosted in sillimanite+K-feldspar anatectic migmatites cropping out twenty kilometres north of the Posada-Asinara Line. The decompressional, granulite facies re-equilibration and the later overprint are widespread at the outcrop scale.

These eclogites are embedded within diatexitic gneisses,

which exhibit different structures depending on the protolith nature and composition. In any case evidence of mobilization of a leucogranitic melt is widespread, resulting in both planar leucosomes arranged into stromatic structures and in dilatant shear zones crosscutting the layering obliquely.

The diatexitites, particularly the stromatic varieties, show mineral assemblages consistent with the occurrence of muscovite dehydration melting below biotite dehydration conditions. The occurrence of relict sillimanite, K-feldspar and biotite at the selvedges within neosome, suggests the reaction:  $\text{Ms} + \text{Pl} + \text{Qtz} = \text{Melt} + \text{Kfs} + \text{Sil} + \text{Bt}$ . Late muscovite, also common in coarse grains within such diatexitite, may be, according to Solar and Brown (2001), the product of  $\text{H}_2\text{O}$  exsolved during the crystallization of the stagnant melt causing the hydration reaction  $\text{Kfs} + \text{Sill} + \text{H}_2\text{O} = \text{Ms} + \text{Qtz}$ .

Within the Gneiss Complex, metabasites occur as:

I- Decametric lenses and boudins within intermediate P metapelites and quartzites affected by late Variscan HT/LP (Asinara Island and Coghinas Lake). No relicts of the eclogite event are evident, and plagioclase+hornblende±biotite largely replace the garnet.

II- Small lenses in the Posada valley phyllonitic belt (Elter, 1987), where decametric bodies of metabasite crop out along the retrograde strike-slip zone. Here, important fluid circulation caused a generalised retrograde re-equilibration to amphibolite and greenschist facies compatibilities.

III- Hectometric slices within staurolite+garnet+kyanite-bearing micaschists and paragneisses in the Anglona region, within the Posada-Asinara Belt (Fig. 2), close to the retrograde shear zone II) but far enough (2.5 km) from its core.

Four samples preserving eclogite paragenetic and textural relicts were selected from the third occurrence.

## ECLOGITES A

### Petrography

In the study outcrop, the eclogite is massive and isotropic to weakly foliated, and at various extent preserves textural and paragenetic evidence of the polyphase evolution from eclogite conditions throughout high-temperature decompression up to low P (garnet-out) amphibolite facies conditions.

The eclogitic assemblage includes garnet+omphacite+colourless Na-Ca amphibole+quartz+ilmenite+rutile+apatite±zoisite±brown mica (Plate 1A). Zircon and allanite occur in sample B1 (Plate 1B) that is also characterised by a relatively high apatite content. Garnet (1-5 mm in size) is zoned, and shows polyphase growth features: the subhedral to lobate pre-kinematic core hosts abundant, randomly oriented micrograins of quartz, omphacite, Na-Ca amphibole, rutile and ilmenite. The rim is inclusion-free and seldom flattened on the foliation, suggesting syn-kinematic growth.

Omphacite only survives as armoured relicts in the garnet, but symplectite pseudomorphs commonly mimic the habit of medium-grained (1-2 mm), subhedral, isoriented omphacite crystals (Plate 2A). Na-Ca amphiboles in part survive as zoned cores within Ca-amphibole; the foliation highlighted by Ca-amphiboles result mimetic by replacement of Na-Ca amphibole partly preserved at their cores. Granoblastic (0.5-2 mm) quartz sparsely occurs (0-5% in volume).

Ilmenites inclusions in garnet show exsolution lamellae of rutile, which are lacking in ilmenites re-equilibrated with amphibole or in the pseudomorphs with orthopyroxene after brown mica (Plate 1A, B). Ilmenite and rutile are widespread in the garnet inclusions, where they coexist with in-

tergrowth textures (Plate 1A). Brown mica (phlogopite?) relicts are hardly preserved.

The decompressional event is characterised by (Plate 2): I) the breakdown of omphacite into symplectite aggregates of diopside+plagioclase±Ca-amphibole±orthopyroxene; II) the development of keliphytic rims of plagioclase+Ca-amphibole on garnet; III) the widespread growth of pinkish-brown Ca-amphibole replacing the colourless Na-Ca amphibole; IV) the growth of orthopyroxene±cummingtonite replacing brown mica (Plate 2B). Cummingtonite is also found rimming the orthopyroxene at the contact with quartz (Plate 1B), or intergrown with Ca-amphibole. Ca-amphibole represents the stable hydrous phase; it mostly developed at the expense of Na-Ca amphibole, and only at minor extent, of omphacite (in symplectite) and garnet (in kelyphites). As dehy-

dration occurs during the breakdown of brown mica to orthopyroxene, likely no or minor exotic input of  $H_2O$ , are required. The diopside+albite pair, in fine-grained symplectite represents metastable equilibria, and towards the boundaries of the former omphacite, it grades towards diopside+plagioclase+Ca-amphibole±orthopyroxene with increasing grain size up to granoblastic mosaic textures. Ilmenite exhibits equilibrium boundaries with Ca-amphibole, whereas rutile is corroded. At the outcrop scale, the most re-equilibrated samples hardly preserve any trace of symplectite.

The retrograde amphibolite facies overprint, poorly developed in the study samples, is recorded by patchy growth along mm to cm-thick areas of fine-grained to acicular green Ca-amphibole, rarely of cummingtonite, in equilibrium with plagioclase and biotite. The alteration of garnet and

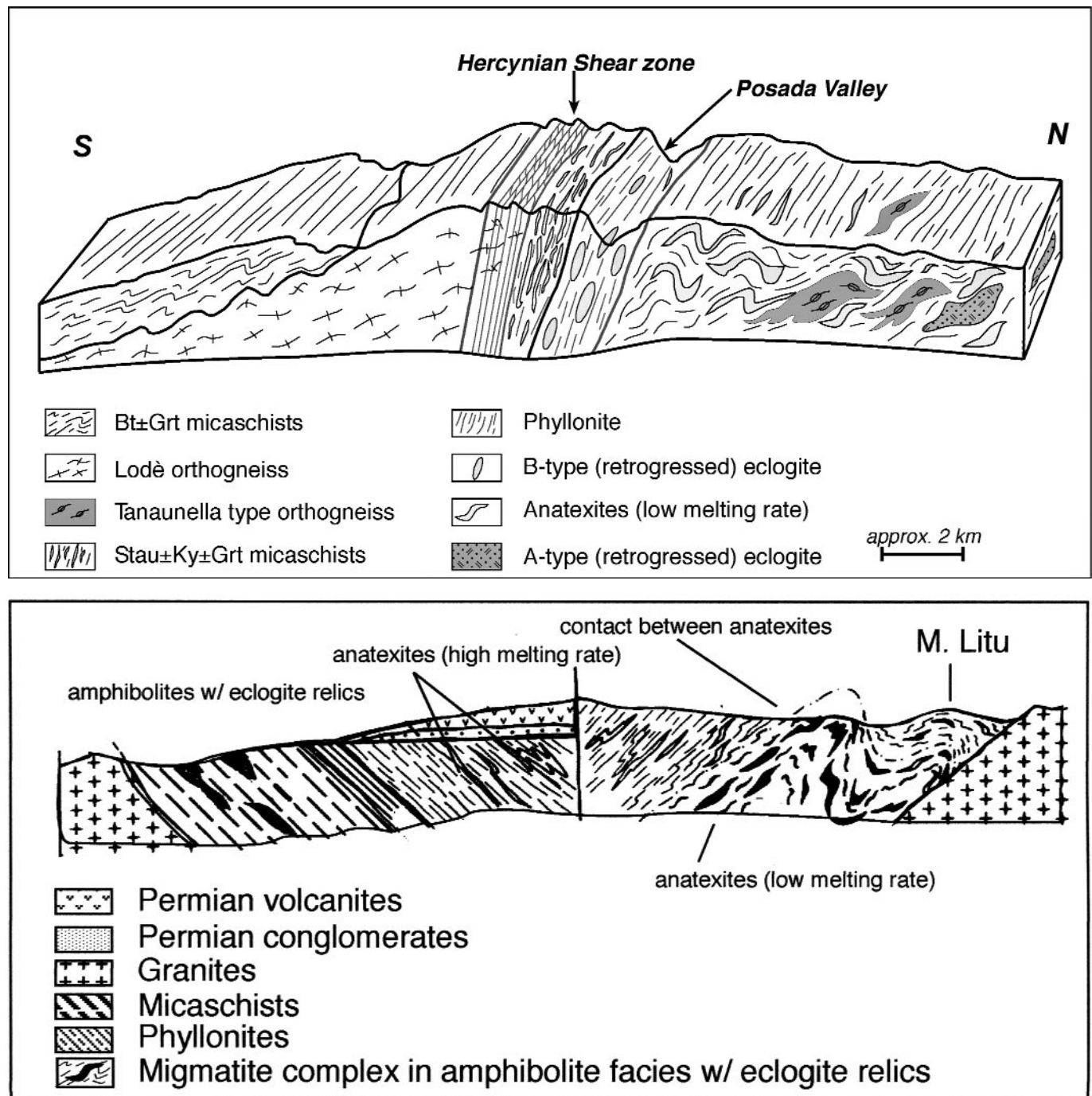


Fig. 2 - A: Geological section across the Posada - Asinara line. B: Geological section at M. Litu: tectonic relationships between eclogite - bearing amphibolites and anatexites.

diopside to Ca-amphibole and biotite suggests a control by local fluid mobilisation.

### Mineral chemistry

#### Garnet

Garnet shows pyrope contents in the range 10-35 mole% (Fig. 3; Table 1), almandine 30-67 mole %, and grossular 2-28 mole%. The contents of spessartine (0.2-4.4 mole%) and andradite (0-1.1 mole%) are low, with appreciable  $TiO_2$  (up to 0.4 wt%) and  $Cr_2O_3$  (up to 0.25 wt%) contents. Pyrope, almandine and grossular contents from different samples broadly correlate with bulk rock chemistry. Concentric zoning is widespread with a relatively homogeneous core, Mg increase and Mn, Ca and Fe decrease in the rim, thus suggesting a prograde trend.

In samples preserving eclogite relicts, the garnet margin (for about 50  $\mu m$ ) is commonly destroyed by the growth of kelyphites. In samples showing near complete decompressional recrystallization, garnet, diopside and Ca-amphibole

developed rational equilibrium boundaries.

#### Pyroxenes

- Na-Ca clinopyroxene.

The Na-Ca clinopyroxene within the garnet cores is omphacite (Fig. 4; Table 2) rarely aegirine augite, with jadeite 12-28 mole%, and aegirine 1-27 mole %.

- Ca-clinopyroxene

Ca-clinopyroxenes from symplectites are diopsides ( $Mg/Mg+Fe$ : 0.64-0.72) with low contents of jadeite (0.4-2.2 mole %) and aegirine (0.0-0.6 mole %) (Table 3). In samples completely re-equilibrated to granulite, the diopside has jadeite contents up to 10 mole %.

- Orthopyroxene

Orthopyroxene (Table 3) shows  $Mg/Mg+Fe$  values in the range 0.38-0.65, with low  $CaO$  (0.5 and 0.88 wt%) and  $Al_2O_3$  (0.11 and 0.80 wt %). Minor  $TiO_2$  (up to 0.23 wt%),  $Cr_2O_3$  (up to 0.20)  $NiO$  (up to 0.45) and  $MnO$  (up to 0.71).

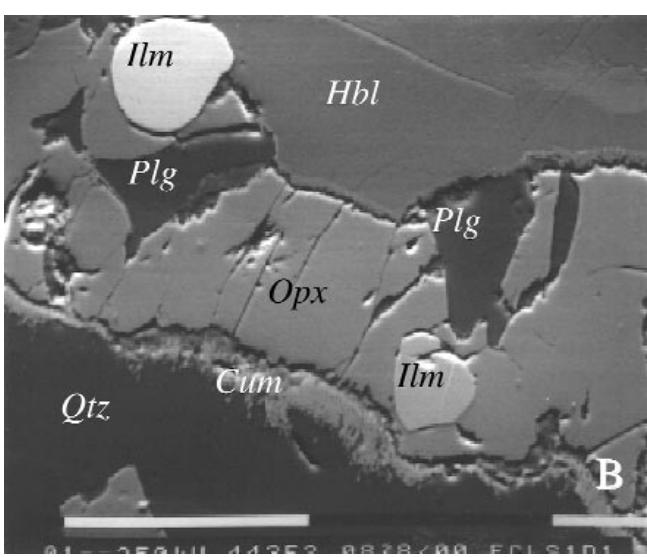
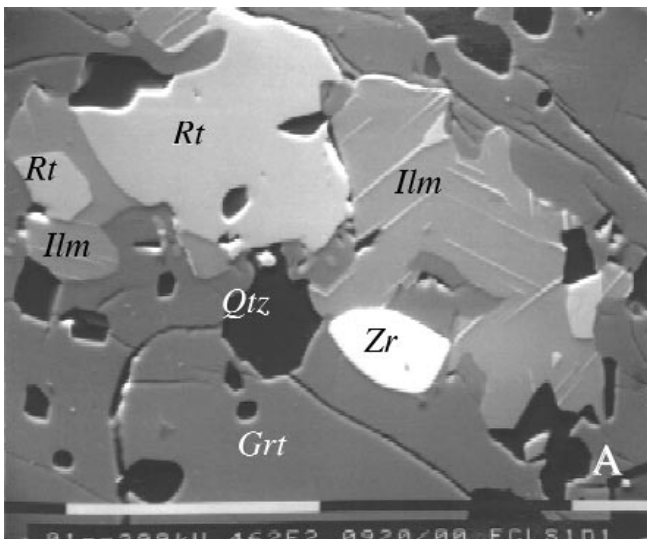


Plate 1 - SEM-BSE photomicrograph, Type A, partially retrogressed, eclogite. A: bar scale is 0.1 mm; coexisting rutile (Rt) and ilmenite (Ilm) inclusions in garnet (Grt) with quartz (Qtz) and zircon (Zr). Trellis texture in ilmenite. B: bar scale is 0.1 mm; orthopyroxene (Opx)+plagioclase (Plg)+ilmenite (Ilm) pseudomorphs on biotite. Cummingtonite (Cum) rim between orthopyroxene and quartz (Qtz). Top left: ilmenite and hornblende (Hbl).

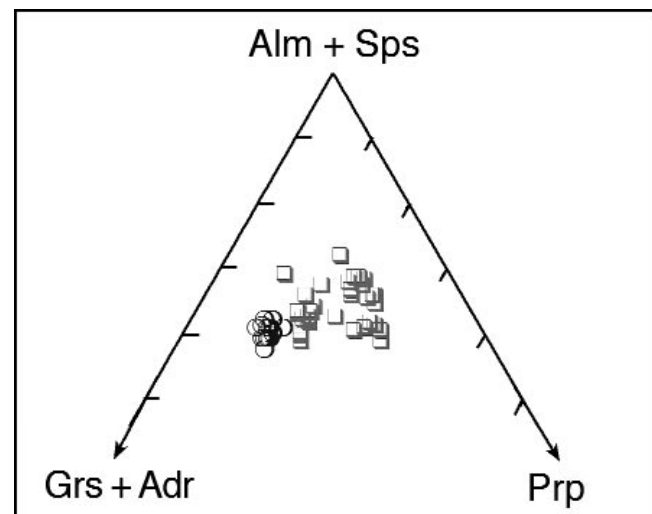


Fig. 3 - Compositional variability of garnets (eclogite facies assemblages). □: A-type eclogites; ○: B-type eclogites.

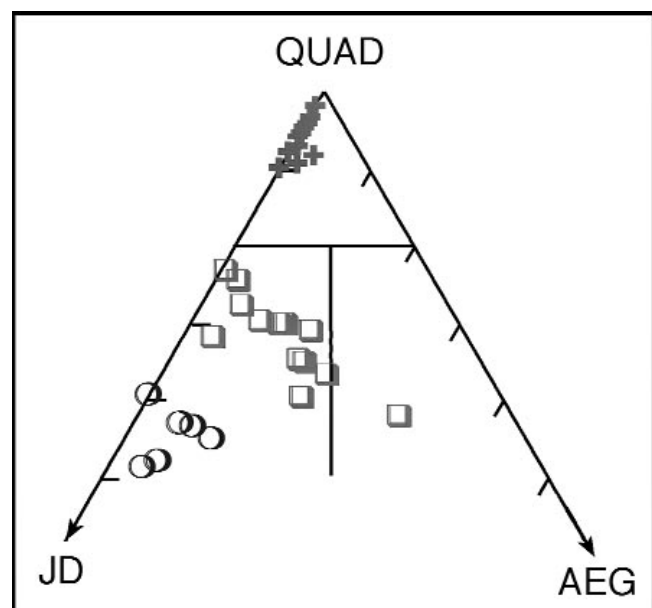


Fig. 4 - Na-Ca clinopyroxene compositions (eclogite facies assemblages) in the Jd-Aeg-QUAD triangle. Nomenclature after Morimoto (1988), compositional fields after Rock (1990). Symbols as in Fig. 3. Crosses: diopside from symplectites (eclogites A).

### Amphiboles

The colourless to greenish Na-Ca amphibole (Table 4), preserved as inclusions in the garnet or as metastable relicts at the core of the Ca-amphibole, is barroisite in the Leake et al. (1997) classification.  $\text{TiO}_2$  is in the range 0.24 and 0.75 wt%.

Compositions of the pinkish-brown Ca-amphibole, stable in the granulite assemblage, range from Mg-hornblende to tschermakite, more rarely is pargasite, without clear relationships with the different textural site; the coarse zoned nematoblastic grains show the largest compositional range.

$\text{TiO}_2$  varies between 1.01 and 1.90 wt%, and the highest contents occur at the contact with ilmenite and/or relict rutile. A tschermakite substitution trend is shown by the  $\text{Al}^{\text{VI}}+\text{Fe}^{3+}+\text{Ti}$  vs.  $\text{Al}^{\text{IV}}$  diagram (Fig. 5A; Table 5). The composition of Ca-amphiboles falls largely in the field of intermediate pressure amphiboles (Laird and Albee, 1981), whereas high-pressure vectors arise for Na-Ca amphiboles. The wide compositional range and partial compositional overlap of Na-Ca and Ca-amphiboles are likely due to incomplete re-equilibration.

The green amphiboles formed during the amphibolite fa-

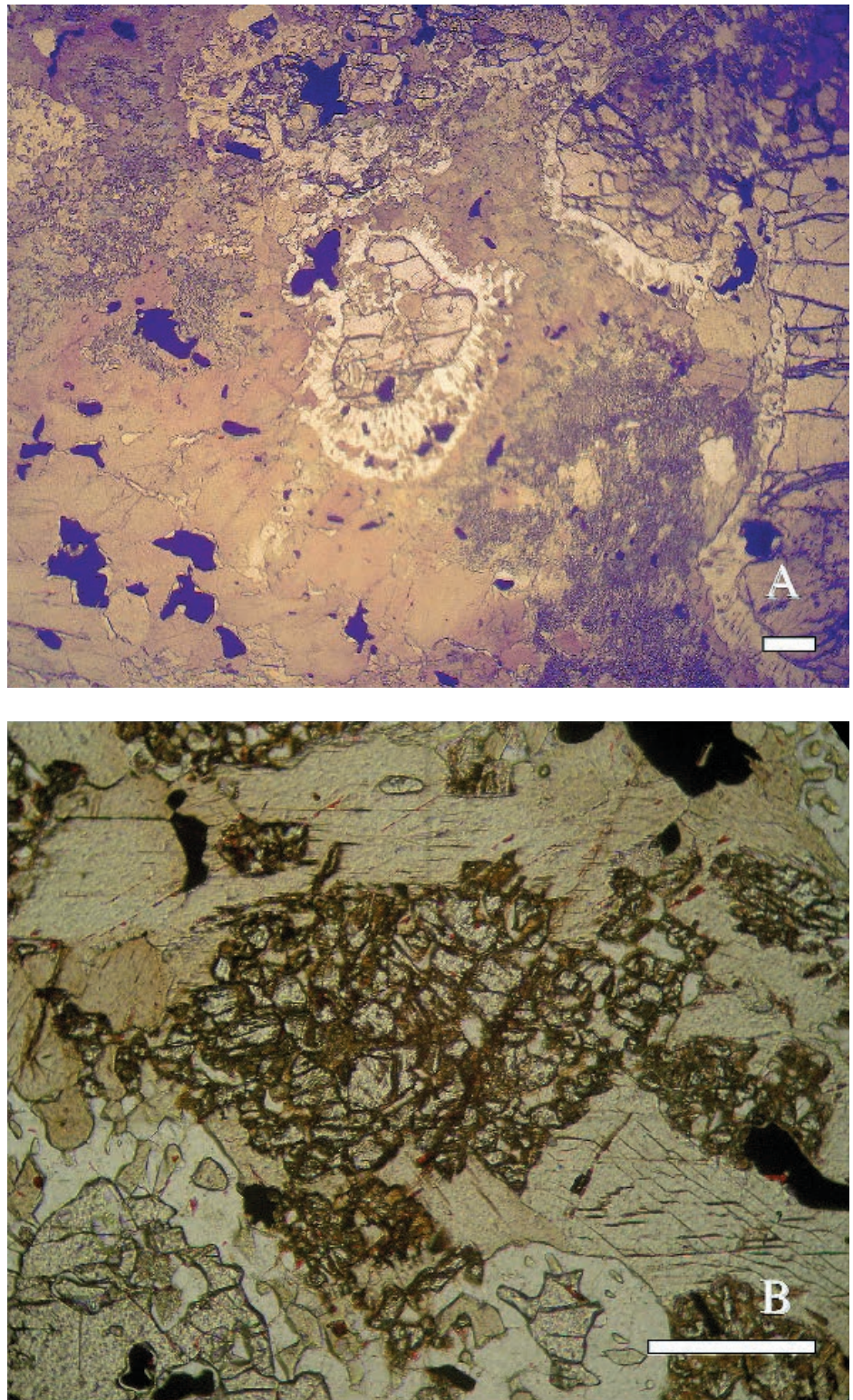


Plate 2 - Photomicrograph of Type A, retrogressed, eclogite. Plane polarised light. A: garnet showing large kelyphite rim. Fine grained diopside - plagioclase symplectite (dark grey) and decussate zoned amphibole II. Scale bar: 1 mm. B: Orthopyroxene+plagioclase+ilmenite+hornblende+cummingtonite pseudomorphic aggregate from biotite. Bottom of photo: kelyphite rims around garnet. Scale bar: 1 mm.

Table 1A - Representative garnet compositions from type B eclogites.

TYPE B Sample Analysis n.	REC2	REC2	REC2	REC2	REC2	REC2	REC2	REC3	REC3	AV35	AV35
	2	3	4	5	6	7	8	1	2	1	2
Texture	Coexisting w/Hbl	Coexisting w/Hbl	Coexisting w/Hbl	Hbl/grt pair	Grt + Na-Ca cpx pair	Grt - hbl pair	Grt	Eclogitic assemblage, coex w/ Na-Ca cpx	Eclogitic assemblage overgrown by retrograde Green Hbl	Na-Ca cpx pair	Na-Ca cpx pair
SiO <sub>2</sub>	38.26	38.27	38.49	38.23	38.25	37.8	38.04	38.28	37.94	37.7	37.4
TiO <sub>2</sub>	0.18	0.18	0.13	0.14	0.03	0.15	0.18	0.07	0.15	0.14	0.24
Cr <sub>2</sub> O <sub>3</sub>	0.26	0.23	0.2	0.18	0.24	0.11	0.19	0.25	0.23	0.19	0.18
Al <sub>2</sub> O <sub>3</sub>	21.24	21.11	21.4	21.03	21.36	21.12	21.25	21.22	21.18	22.13	22.04
Fe <sub>2</sub> O <sub>3</sub>	1.09	1.04	0.50	1.99	1.23	2.19	0.93	1.11	1.24	0.24	0.94
FeO	25.93	26.04	26.84	26.13	26.99	26.17	26.27	26.81	25.95	26.05	25.39
MnO	0.63	1.35	0.87	0.48	0.34	0.61	1.47	0.69	0.46	0.95	0.57
MgO	3.06	2.65	2.61	3.12	3.32	3.08	2.61	2.90	2.88	2.46	2.76
NiO	0.00	0.13	0.14	0.16	0.06	0.18	0.02	0.02	0.03	0.00	0.09
CaO	10.75	10.6	10.55	10.45	9.65	10.01	10.22	10.26	10.77	10.71	10.85
Na <sub>2</sub> O	0.00	0.00	0.00	0.00	0.00	0.00	0.00	0.00	0.00	0.00	0.00
K <sub>2</sub> O	0.04	0.03	0.04	0.04	0.03	0.02	0.04	0.00	0.04	0.03	0.02
Total	101.44	101.62	101.77	101.95	101.5	101.44	101.22	101.6	100.87	100.59	100.48
Si	2.9774	2.9836	2.9929	2.968	2.9767	2.9523	2.9779	2.9818	2.9718	2.9574	2.9344
Ti	0.0105	0.0106	0.0076	0.0082	0.0018	0.0088	0.0106	0.0041	0.0088	0.0083	0.0142
Cr	0.016	0.0142	0.0123	0.011	0.0148	0.0068	0.0118	0.0154	0.0142	0.0118	0.0112
Al	1.9481	1.9391	1.9612	1.9242	1.9591	1.9441	1.9606	1.9481	1.9553	2.0466	2.0381
Fe <sup>3+</sup>	0.0641	0.0609	0.0295	0.1163	0.0722	0.1287	0.0548	0.0648	0.0731	0.0146	0.0556
Fe <sup>2+</sup>	1.6872	1.6975	1.7451	1.6964	1.7566	1.7093	1.7200	1.7461	1.7002	1.7087	1.6662
Mn	0.0415	0.0891	0.0573	0.0316	0.0224	0.0404	0.0975	0.0455	0.0305	0.0631	0.0379
Mg	0.3549	0.3079	0.3025	0.361	0.3851	0.3586	0.3045	0.3367	0.3362	0.2876	0.3228
Ni	0.000	0.0082	0.0088	0.01	0.0038	0.0113	0.0013	0.0013	0.0019	0.000	0.0057
Ca	0.8963	0.8854	0.8789	0.8692	0.8046	0.8377	0.8572	0.8563	0.9039	0.9001	0.9121
Na	0.000	0.000	0.000	0.000	0.000	0.000	0.000	0.000	0.000	0.000	0.000
K	0.004	0.003	0.004	0.004	0.003	0.002	0.004	0.000	0.004	0.003	0.002
Grossular	0.254	0.253	0.269	0.224	0.226	0.21	0.248	0.245	0.255	0.286	0.269
Almandine	0.565	0.569	0.584	0.573	0.591	0.58	0.577	0.585	0.572	0.577	0.567
Pyrope	0.119	0.103	0.101	0.122	0.13	0.122	0.102	0.113	0.113	0.097	0.11
Spessartite	0.014	0.03	0.019	0.011	0.008	0.014	0.033	0.015	0.01	0.021	0.013
Andradite	0.032	0.031	0.015	0.059	0.036	0.066	0.028	0.033	0.037	0.007	0.028
Uvarovite	0.008	0.007	0.006	0.006	0.007	0.003	0.006	0.008	0.007	0.006	0.006
Ti-Al Garnet	0.003	0.004	0.002	0.002	0.000	0.003	0.003	0.002	0.002	0.003	0.006
Na-Ti Garnet	0.004	0.003	0.004	0.004	0.002	0.002	0.004	0.000	0.004	0.003	0.002

Textural features referred to in the table.

cies overprint are Mg-hornblende with low TiO<sub>2</sub> (0.01-0.95 wt%) sometimes grading to actinolite.

Cummingtonite intergrown with Ca-amphibole shows high Mg contents (Mg/Mg+Fe = 0.8-1.00) and low Al and Ca (Al = 0.05-0.032 a.p.f.u. Ca = 0.79-0.09 a.p.f.u.). Cummingtonite coexisting with orthopyroxene is too fine grained for reliable analysis.

#### Plagioclase

Plagioclase from symplectites shows a continuous compositional range from near pure albite to andesine (An: 12-41 mole %). Andesine plagioclase also occurs in kelyphites and interstitial to Ca-amphibole. The K<sub>2</sub>O content varies between 0.1-0.5 wt%. Plagioclase in retrograde amphibolite facies aggregates is oligoclase.

#### Biotite

Biotites replacing garnet, with plagioclase and green amphibole have Mg# between 0.4-0.6, and relatively high Al<sub>2</sub>O<sub>3</sub> (15-16 wt%) and TiO<sub>2</sub> (2.06-2.80 wt%).

#### Ilmenite

The composition is homogeneous close to that of the pure end member except for appreciable contents of Mn (0.74 < MnO < 1.70), Cr<sub>2</sub>O<sub>3</sub> (up to 0.18 wt%), NiO (up to 0.69 wt %) and CaO (up to 0.43 wt%).

## ECLOGITES B

### Petrography

Re-crystallization to amphibolite facies compatibilities is pervasive throughout the outcrop so that mineral phases of

the eclogite assemblage are only preserved in rare samples as armoured relicts in the garnet (Plate 3).

Coarse to medium-grained (0.5-4 mm), subhedral to amoeboid garnets include abundant, randomly or poorly oriented quartz, clinozoisite, omphacite, Na-Ca amphibole, rutile, ilmenite, apatite.

Fine-grained symplectites of clinopyroxene+plagioclase±Ca-amphibole (Plate 3B) preserving the habit and shape of pristine medium-grained, subhedral omphacite grains are found in amphibole aggregates or overgrown by garnet. Decussate to nematoblastic green Ca-amphiboles rarely preserve cores of colourless Na-Ca amphibole and co-exist with plagioclase, clinozoisite, titanite and rare brown mica (Plate 3A, B). Relics of a syn-eclogite S<sub>1</sub> evidenced by flattened garnets or isoriented omphacite ghosts, can be detected. The orientation of Ca-amphiboles and garnet fracturing evidence a post-eclogitic schistosity, parallel to the S<sub>2</sub> of the host gneisses. Locally, plagioclase+Ca-amphibole+biotite replace garnet whereas titanite overgrows rutile and ilmenite. In the host paragneisses, garnet, kyanite, staurolite, biotite and muscovite preserve the folded S<sub>1</sub> schistosity, whereas biotite, muscovite and plagioclase recrystallise on the S<sub>2</sub>. A later mylonitic phase, associated with chloritisation, is widespread.

### Mineral chemistry

#### Garnet

In spite of the relatively wide bulk rock compositional range (Mg# 27.4-34.4), garnet has homogenous composition (Fig. 3; Table 5) and lacks appreciable zoning. The almandine content is high (55-60 mole %), grossular is in the

Table 1B - Representative garnet compositions from type A eclogites.

Textural features referred to in the table.

Table 2 - Representative compositions of Na-Ca-clinopyroxene from type A eclogites.

TYPE A		TYPE B												
Sample Analysis n.	Texture	ES2-2	ES2-2	ES2-2	ES2-2	ES2-2	ES2-1	ES2-1	ES2-1	REC 3	REC 2	REC 2	REC 2	AV35
ES2-2	1	ES2-2	4	ES2-2	5	ES2-2	7	ES2-2	8	REC 3	1	REC 2	2	1
SiO <sub>2</sub>	Eclogitic assemblage; pair w/ grt	52.47	52.62	52.3	52.16	52.05	53.05	53.39	53.56	52.67	55.01	54.47	54.98	54.82
TiO <sub>2</sub>		0.14	0.15	0.21	0.1	0.12	0.18	0.09	0.2	0.2	0.1	0.08	0.13	0.15
Cr <sub>2</sub> O <sub>3</sub>		0.28	0.21	0.27	0.26	0.31	0.27	0.25	0.23	0.22	0.32	0.34	0.30	0.27
Al <sub>2</sub> O <sub>3</sub>		6.4	6.21	6.04	6.14	6.42	7.16	6.66	7.08	9.07	10.60	9.70	11.38	10.12
Fe <sub>2</sub> O <sub>3</sub>		2.73	3.48	0.95	0.29	4.95	1.26	6.02	1.67	0.00	1.86	1.93	1.41	3.50
FeO		6.99	6.74	9.84	4.68	4.68	7.9	2.91	9.65	8.41	5.95	5.51	5.22	2.88
MnO		0.13	0.11	0.17	0.13	0.06	0.14	0.04	0.21	0.25	0.15	0.11	0.04	3.65
MgO		8.57	9.04	8.89	9.69	8.95	8.23	8.82	9.12	6.68	6.04	7.36	6.21	8.53
NiO		0.95	0.08	0.14	0.13	0.12	0.23	0.24	0.09	0.34	0.33	0.35	0.22	0.14
CaO		16.33	16.48	16.65	16.8	16.37	16.14	15.76	15.36	14.24	14.48	13.41	13.72	14.46
Na <sub>2</sub> O		3.96	4.03	3.25	3.09	4.64	4.32	5.36	3.68	5.60	6.04	6.79	6.19	5.98
KO		0.09	0.07	0.11	0.09	0.08	0.12	0.06	0.07	0.03	0.03	0.08	0.05	0.09
Total		99.04	99.22	98.81	97.69	99.76	99.34	99.76	100.03	100.07	100.02	101.18	100.16	100.92
Si		1.9582	1.955	1.9678	1.9518	1.9752	1.959	1.9472	2.0062	1.9728	1.9744	1.9755	1.9469	1.9541
Ti		0.0039	0.0042	0.0059	0.0028	0.0033	0.005	0.0025	0.0056	0.0049	0.0027	0.0022	0.0003	0.0004
Cr		0.0083	0.0062	0.008	0.0078	0.009	0.0079	0.0072	0.0067	0.0097	0.0062	0.0085	0.0037	0.0082
Al		0.2815	0.2719	0.2673	0.273	0.2784	0.2871	0.3122	0.3085	0.3898	0.4525	0.4093	0.4819	0.4252
Fe <sup>2+</sup>		0.0768	0.0972	0.0267	0.0883	0.1371	0.035	0.1656	0.0463	0.000	0.0508	0.0521	0.0382	0.0677
Fe <sup>3+</sup>		0.2182	0.2095	0.309	0.2779	0.1441	0.2443	0.0889	0.2984	0.2565	0.1803	0.165	0.1568	0.0855
Mn		0.0035	0.0041	0.0054	0.0042	0.0019	0.0044	0.0012	0.0066	0.0077	0.0046	0.0033	0.0012	0.1088
Mg		0.4767	0.5006	0.4976	0.5449	0.4908	0.4538	0.4808	0.5025	0.3631	0.3261	0.3928	0.4051	0.4532
Ni		0.0224	0.0042	0.0039	0.0036	0.0042	0.0068	0.0071	0.0027	0.010	0.0096	0.002	0.0064	0.002
Ca		0.653	0.656	0.6699	0.6791	0.6453	0.6398	0.6176	0.6084	0.5564	0.5204	0.5593	0.5282	0.5523
Na		0.2865	0.2903	0.2366	0.2226	0.331	0.3099	0.3801	0.2638	0.306	0.467	0.4193	0.473	0.4133
K		0.0043	0.0033	0.0053	0.0043	0.0038	0.0057	0.0028	0.0033	0.0023	0.0014	0.0037	0.0023	0.0041
Wo		0.308	0.308	0.32	0.325	0.300	0.31	0.29	0.281	0.278	0.249	0.268	0.252	0.255
En		0.253	0.251	0.251	0.274	0.247	0.23	0.244	0.253	0.187	0.168	0.201	0.169	0.229
Fs		0.109	0.105	0.139	0.139	0.105	0.123	0.127	0.144	0.128	0.149	0.128	0.143	0.054
Ag		0.077	0.097	0.077	0.077	0.098	0.137	0.035	0.166	0.046	0.051	0.052	0.078	0.068
Id		0.214	0.196	0.215	0.222	0.198	0.228	0.217	0.221	0.198	0.217	0.221	0.371	0.336

Table 3 - Representative compositions of Ca-clinopyroxene and orthopyroxene from type A eclogites.

Sample Analysis n.		EST1A	EST1A	EST2-1	EST2-1	ES2-1	ES2-1	Sample Analysis n.	ES2-1	Texture	Symp	Coex Hb in symplectite	Coex Hb in symplectite	ES1D1	ES1D1	ES1D1	ES1B1	ES1B1	ES1B1	ES2-2
Texture	In symplectite	In symplectite	In symplectite cpx coronitic on quartz	In symplectite	In symplectite	In symplectite	In symplectite													
SiO <sub>2</sub>		51.99	51.5	52.06	51.65	51.2 SiO <sub>2</sub>	50.64	50.40	51.11	51.23	51.90	51.42	51.59	55.11	50.14					
TiO <sub>2</sub>	0.05	0.33	0.06	0.25	0.34	0.28	0.32	0.09 TiO <sub>2</sub>	0.05	0.08	0.00	0.13	0.23	0.11	0.13	0.21	0.17	0.21	0.17	
Cr <sub>2</sub> O <sub>3</sub>	0.29	0.31						0.32 Cr <sub>2</sub> O <sub>3</sub>	0.13	0.04	0.10	0.12	0.11	0.15	0.21	0.23	0.16	0.23	0.16	
Al <sub>2</sub> O <sub>3</sub>	0.66	2.96	0.89	1.74	0.00	0.25	1.87	Al <sub>2</sub> O <sub>3</sub>	0.27	0.31	0.23	0.46	0.51	0.73	0.47	0.62	1.34			
FeO <sub>x</sub>	0.99	0.00	0.25	0.00	0.00	0.00	0.00	FeO <sub>x</sub>	0.58	1.60	1.87	0.46	0.46	2.19	0.47	0.23	1.68	0.00	1.68	
FeO	8.86		10.06	11.25	11.39	10.76	10.76	FeO	35.77	31.05	26.1	25.7	27.35	28.34	28.06	28.54	28.43			
MnO	0.15	0.18	0.28	0.34	0.24	0.24	0.24	MnO	0.72	0.71	0.46	0.48	0.54	0.48	0.59	0.38	0.53			
MgO	12.98	11.42	11.67	11.32	11.51	12.59	12.59	MgO	15.69	18.76	19.06	18.71	17.86	17.88	20.43	16.76				
NiO	0.13	0.31	0.27	0.17	0.15	0.15	0.15	NiO	0.18	0.07	0.52	0.45	0.41	0.41	0.29	0.25				
CaO	23.11	21.65	22.91	21.99	22.67	22.67	22.67	CaO	0.77	0.64	0.48	0.52	0.54	0.37	0.5	0.72	0.64			
NaO	0.02	0.15	0.00	0.00	0.25	0.00	0.00	NaO	0.00	0.00	0.00	0.00	0.00	0.00	0.00	0.00	0.00			
K <sub>2</sub> O	0.08	0.1	0.12	0.07	0.07	0.07	0.07	K <sub>2</sub> O	0.07	0.00	0.00	0.04	0.11	0.02	0.01	0.06	0.07			
Total	99.31	98.97	100.1	99.45	98.88	98.88	98.88	Total	101.53	100.83	99.63	100.38	100.47	100.35	100.3	98.59	100.17			
Si	1.968	1.963	1.972	1.966	1.958	1.9834	1.9834	Si	1.9666	1.9662	1.9537	1.9762	1.9719	1.9794	1.9794	2.0052	1.939			
Ti	0.0014	0.0095	0.0017	0.0072	0.0026	Ti	0.0015	Ti	0.0023	0.0000	0.0037	0.0066	0.0032	0.0038	0.0006	0.0049				
Cr	0.0087	0.0093	0.0102	0.0084	0.0097	Cr	0.0004	Cr	0.0012	0.0003	0.0036	0.0033	0.0045	0.0045	0.0064	0.0049	0.0049			
Al	0.0294	0.133	0.3937	0.0781	0.0843	Al	0.0125	Al	0.0142	0.0104	0.0207	0.0104	0.0229	0.033	0.0213	0.0278	0.0611			
Fe <sup>3+</sup>	0.0283	0.0000	0.0071	0.0000	0.0000	Fe <sup>3+</sup>	0.0000	Fe <sup>3+</sup>	0.0171	0.0466	0.0541	0.0629	0.0135	0.0132	0.0066	0.0000	0.049			
Fe <sup>2+</sup>	0.2804	0.3207	0.3564	0.3626	0.3442	Fe <sup>2+</sup>	1.1772	1.0886	0.8397	0.8196	0.8708	0.8088	0.9005	0.6531	0.9195					
Mn	0.0048	0.0058	0.0099	0.011	0.078	Mn	0.024	Mn	0.0234	0.0234	0.015	0.0155	0.0174	0.0156	0.0192	0.0174				
Mg	0.7324	0.6489	0.6591	0.6424	0.6562	Mg	0.7385	Mg	0.7082	0.7057	10.757	10.834	10.619	10.225	11.577	0.9662				
Ni	0.004	0.0059	0.0082	0.0046	0.0046	Ni	0.0052	Ni	0.0022	0.0161	0.0138	0.0000	0.0126	0.0194	0.0089	0.0078				
Ca	0.9373	0.8842	0.9301	0.897	0.929	Ca	0.0325	Ca	0.0266	0.0198	0.0212	0.022	0.0152	0.0206	0.0293	0.0265				
Na	0.0015	0.0111	0.000	0.0185	0.0000	Na	0.0000	Na	0.0000	0.0000	0.0000	0.0000	0.0000	0.0000	0.0000	0.0000				
K	0.0039	0.0049	0.0058	0.0034	0.0034	K	0.0035	K	0.0000	0.0000	0.0019	0.0053	0.0001	0.0005	0.0029	0.0035				
Wo	0.455	0.428	0.432	0.435	0.445	En	0.37	En	0.452	0.543	0.544	0.527	0.51	0.516	0.583	0.473				
En	0.368	0.329	0.334	0.324	0.33	Fs	0.585	Fs	0.501	0.418	0.406	0.432	0.449	0.446	0.327	0.446				
Fs	0.14	0.16	0.178	0.181	0.172	W <sub>o</sub>	0.016	W <sub>o</sub>	0.013	0.011	0.011	0.008	0.01	0.01	0.015	0.013				
Aeg	0.005	0.000	0.006	0.000	0.000	Ca	0.003	Ca	0.000	0.000	0.000	0.000	0.000	0.000	0.000	0.000				
Ia	0.000	0.016	0.000	0.000	0.000	Ca	0.000	Ca	0.000	0.000	0.000	0.000	0.000	0.000	0.000	0.000				

Table 4 - Representative compositions of Na-Ca amphiboles from types A and B eclogites.

Sample Analysis n.	Texture	TYPE A				TYPE B				Core-Rim boundary	Rim
		EST1D1	EST1B1	EST1B1	EST1B1	REC2	REC2	REC2	AV35		
SiO <sub>2</sub>	Granulitic assemblage	48.72	44.47	47.52	46.50	49.75	50.06	52.98	47.74	52.25	46.08
TiO <sub>2</sub>	Red hbl in Grt in contact w/lm	0.90	1.90	1.02	1.11	1.25	1.01	0.27	0.49	0.50	0.55
Cr <sub>2</sub> O <sub>3</sub>		0.28	0.24	0.17	0.07	0.23	0.24	0.17	0.17	0.15	0.14
Al <sub>2</sub> O <sub>3</sub>		5.80	11.57	8.80	9.56	5.04	5.18	3.99	7.35	11.18	11.62
Fe <sub>2</sub> O <sub>3</sub>		15.30	11.27	15.97	15.54	19.26	18.43	12.69	18.44	6.06	12.09
FeO		0.00	2.98	0.00	0.00	0.00	0.00	2.80	0.00	9.55	4.66
MnO		0.30	0.14	0.22	0.22	0.38	0.28	0.18	0.25	0.19	0.13
MgO		15.27	13.29	15.02	14.36	14.52	17.62	15.38	14.00	10.95	12.37
NiO		0.42	0.21	0.16	0.33	0.14	0.16	0.19	0.14	0.30	0.00
CaO		9.62	9.69	8.78	9.42	7.83	5.18	9.81	8.10	9.26	9.59
Na <sub>2</sub> O		0.68	2.29	0.69	0.46	0.00	0.46	0.70	0.97	2.77	2.28
K <sub>2</sub> O		0.25	0.30	0.32	0.26	0.25	0.36	0.15	0.40	0.17	0.34
H <sub>2</sub> O		2.11	2.09	2.16	2.13	2.15	2.25	2.15	2.20	2.16	2.12
Total		99.65	100.45	100.83	99.95	100.80	101.23	101.53	103.76	100.93	101.97
Si		6.936	6.367	6.606	6.556	6.926	6.667	7.390	6.978	6.843	6.522
Mg		3.240	2.836	3.112	3.018	3.013	3.498	3.198	2.841	2.339	2.610
Al		0.973	1.953	1.442	1.589	0.827	0.813	0.027	0.018	0.019	1.939
Fe <sup>3</sup>		1.639	1.215	1.671	1.648	2.018	1.847	1.332	1.889	0.653	1.288
Fe <sup>2</sup>		0.357						0.327		1.145	0.552
Ti		0.096	0.205	0.107	0.118	0.131	0.101	0.656	1.179	1.889	0.059
Cr		0.032	0.027	0.019	0.008	0.025	0.025	0.028	0.050	0.054	0.016
Ni		0.048	0.024	0.018	0.037	0.016	0.017	0.021	0.015	0.035	0.009
Mn		0.036	0.017	0.026	0.045	0.032	0.032	0.021	0.029	0.023	0.016
Ca		1.467	1.486	1.308	1.423	1.168	0.739	1.466	1.182	1.422	1.454
Na <sub>M4</sub>		0.188	0.514	0.186	0.126	0.119	0.189	0.256	0.578	0.186	0.546
Total M4		1.655	2.000	1.494	1.549	1.168	0.858	1.655	1.438	2.000	2.000
Na <sub>tot</sub>		0.188	0.636	0.186	0.126	0.119	0.189	0.256	0.770	0.186	0.626
Na <sub>A</sub>		0.045	0.055	0.057	0.047	0.044	0.061	0.027	0.070	0.031	0.080
Total A		0.045	0.055	0.057	0.047	0.044	0.061	0.027	0.070	0.041	0.061
OH		2.000	Barroisite	Barroisite	Barroisite	Barroisite	Barroisite	Barroisite	Barroisite	2.000	0.142
Name		(Leake et al. 1997)	Barroisite (low Si)							Barroisite	2.000
										Barroisite	Barroisite

Table 5 - Representative compositions of Ca amphiboles from types A and B eclogites.

range 21-27 mole% and pyrope is relatively low (10-13 mole %). Spessartine (1-3 mole %) and andradite (1-6 mole %) are low. Minor elements are  $\text{TiO}_2$  (up to 0.22 wt %) and  $\text{Cr}_2\text{O}_3$  (up to 0.25 wt%).

#### *Pyroxenes*

Na-Ca clinopyroxenes from garnet inclusions are omphacites (Fig. 4; Table 2) with jadeite in the range 33-43 mole %, and low aegirine contents (0-9 mole %), without correlation with the bulk rock composition.

Ca-clinopyroxenes in symplectites are diopsides with

very low jadeite (1-2.5 mole %) and aegirine (0.0-1.3 mole%).

#### *Amphiboles*

Colourless Na-Ca amphiboles (Table 4) are barroisites (Leake et al., 1997) showing low  $\text{TiO}_2$  content (0.14-0.55 wt%). Ca-amphiboles are Mg-hornblendes with wide  $\text{TiO}_2$  range (0.04-1.39 wt%; Fig. 5B).

#### *Feldspars*

Plagioclase coexisting with Ca-amphibole has anorthite

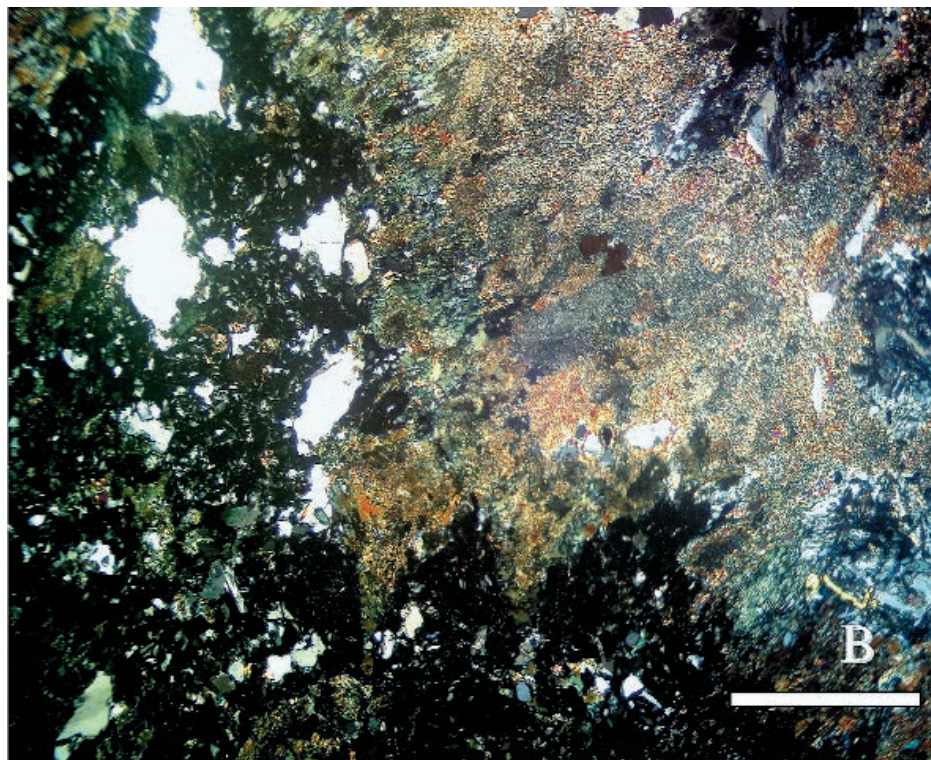
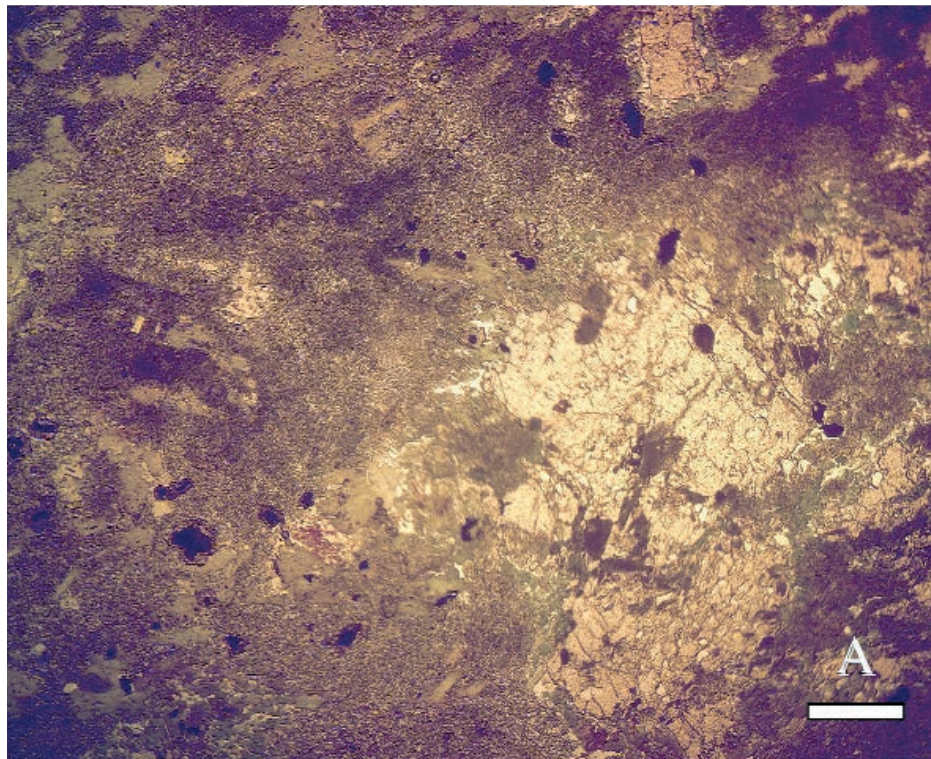


Plate 3 - Photomicrograph of Type B, retrogressed, eclogite. Plane polarised light. A: Unzoned poikiloblastic garnet affected by later deformation. Very fine grained (dark grey) symplectite aggregates preserve the shape of ghost omphacite. Coarse zoned amphiboles II (light grey). Opaque is ilmenite partially surrounded by titanite. Scale bar: 1 mm. B: detail of ghost subhedral omphacite in aggregates of amphibole II. Scale bar: 1 mm.

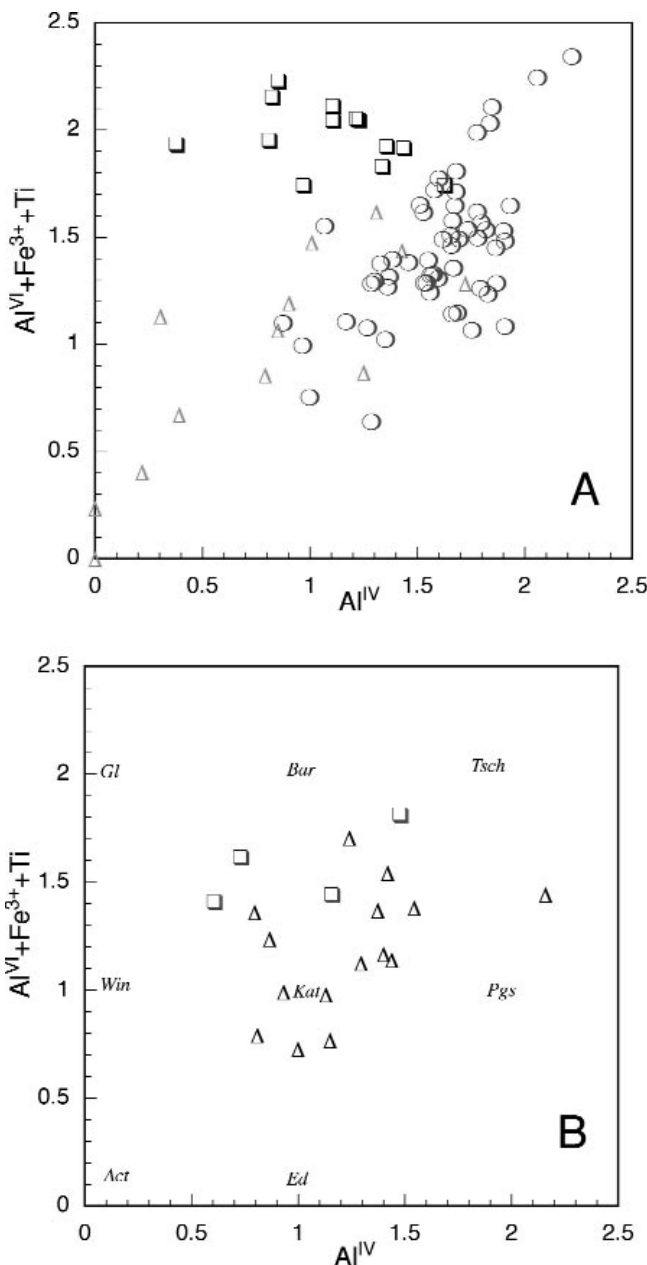


Fig. 5 -  $\text{Al}^{\text{IV}}$  -  $\text{Al}^{\text{VI}} + \text{Fe}^{3+} + \text{Ti}$  for Ca- and Na-Ca-amphiboles. Symbols as in Fig. 3. A: A-type eclogites. B: B-type eclogites.

contents between 22 and 30 mole% and  $\text{K}_2\text{O}$  in the range 0.1-0.2 wt%. Rare interstitial K-feldspar coexists with plagioclase. Anorthite grains ( $\text{An} > 90$  mole %) occur with quartz as inclusions in garnet.

#### Epidote

Clinozoisite inclusions in garnet, have relatively low pistacite ( $\text{Ps}_{11-17}$ ) contents solutions, and likely represent equilibrium compositions with garnet. However, a partial re-equilibration cannot be excluded. Epidotes developed in amphibolite facies assemblages have higher pistacite contents ( $\text{Ps}_{25-33}$ ).

#### Ilmenite

Ilmenite has homogeneous compositions, close to the pure end-member, with low  $\text{MnO}$  (0.79-2.78 wt%),  $\text{Cr}_2\text{O}_3$  (up to 0.27 wt%),  $\text{NiO}$  (up to 0.89 wt %), and  $\text{CaO}$  (up to 0.31 wt%).

## GEOTHERMOBAROMETRIC CONSTRAINTS

Thermobarometric evaluations for the eclogite stage are based on the Fe-Mg exchange in garnet – omphacite pairs as calibrated by Ellis and Green (1979), Ganguly (1979), Krogh (1988), Dahl (1980), Pattison and Newton (1989), Ai (1994) and on jadeite mole fraction of omphacite in the presence of quartz (Holland, 1983; Essene and Fyfe, 1967). Compositions of omphacite inclusions combined with adjacent garnet are considered in equilibrium and suitable for PT evaluation. Furthermore, solutions to combinations of the phase equilibria were obtained by application or iteration of the Thermobarometry 2.1 program (Spear and Kohn, 1999; [http://ees2.geo.rpi.edu/MetaPetaRen/Frame\\_software.html](http://ees2.geo.rpi.edu/MetaPetaRen/Frame_software.html)).

In eclogites A, omphacite grains occur at the garnet core, as the zoning suggests a prograde trend, the analysed pairs probably represent an early eclogite stage at PT conditions lower than the metamorphic peak. In eclogites B, omphacite inclusions are randomly distributed and no apparent zoning is present in the garnet. The amphibolite facies thermobaric conditions were estimated by the hornblende-plagioclase geothermometry (Blundy and Holland, 1990; Holland and Blundy, 1994).

#### Eclogites A

The calibrations, calculated for six omphacite-host garnet pairs, provide temperatures in the range 690°-760°C for minimum pressure  $\approx 1.3$  GPa, consistent with the isopleths of jadeite in omphacite. Underestimated temperatures arise from the Pattison and Newton (1989) calibration. Pyroxene compositions in the solvus omphacite P2/n - augite C2/c (Carpenter, 1980) accord with temperatures in excess of 700°C. Temperatures about 600°-700°C, and pressures 1.3-1.5 GPa were estimated for the eclogitic stage in metabasites from Punta de li Tulchi and Punta Tittinosu (Palmeri et al., 1997; Franceschelli et al., 1998).

The omphacite breakdown and the coexistence of clinopyroxene, orthopyroxene and plagioclase with garnet and amphibole indicate transition to conditions between high temperature amphibolite and granulite facies. Temperatures exceeding 700°C, suggested by coexisting plagioclase-Ca-amphibole pairs (Blundy and Holland, 1990) for pressures below 0.8-1.0 GPa are consistent with a virtually adiabatic rise during the exhumation phase. The garnet - clinopyroxene geothermometer (Powell, 1985) in well re-equilibrated samples yields temperatures about 700°C. The replacement of brown mica by orthopyroxene and cummingtonite corresponds to the equilibrium  $\text{Phl} + 4\text{En} + 4\text{Qtz} \leftrightarrow \text{Cum} + \text{Or}$ , where cummingtonite is stable at the considered temperatures for  $P < \approx 0.8$  GPa (Evans and Ghiorso, 1995). Mg-cummingtonite is stable with orthopyroxene+quartz for temperatures  $\geq 750^\circ\text{C}$  and pressures between 1.0-0.5 GPa (Ghiorso et al., 1995; Evans and Ghiorso, 1995).

K-feldspar from the mica breakdown was never found, likely due to  $\text{K}_2\text{O}$  solution in the coexisting plagioclase.

The amphibolite facies overprint is poorly developed in the study samples; temperatures in the range 550°C-650°C and pressures 0.3-0.7 GPa are suggested by Palmeri et al. (1997).

#### Eclogites B

The thermometric calibrations based on five omphacite-host garnet pairs yield temperatures in the range 610°-

700°C for pressures  $\leq 1.5$  GPa, based on the jadeite content. Higher temperatures obtained with the Ganguly (1979) calibration are considered as overestimated.

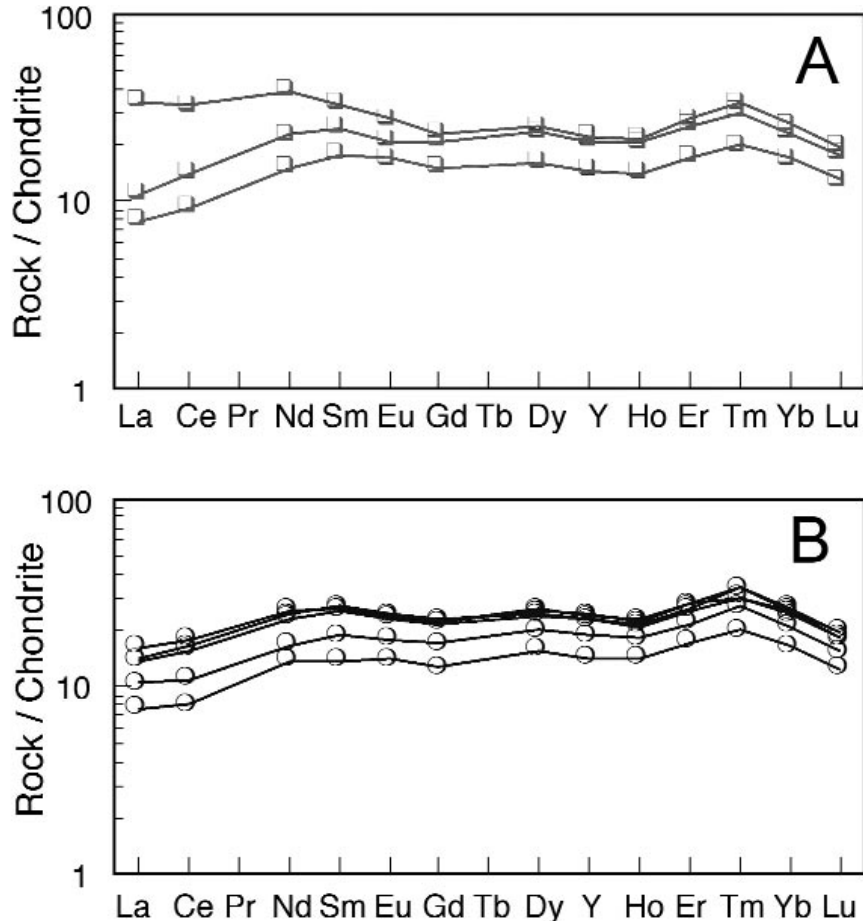
Thermometric evaluations in the considered range are consistent with the biotite+muscovite+garnet+kyanite+staurolite assemblage in the host paragneisses, moreover the lack of anatexic processes allows to exclude temperatures largely exceeding 650°C.

The occurrence of An-rich plagioclase and quartz as inclusions in garnet can be interpreted as due to dehydration reactions within a confined chemical domain, such as clinzoisite+quartz = anorthite+garnet+fluids, zoisite+quartz = anorthite+grossular+fluids and epidote+quartz = anorthite+grossular/andradite+hematite+ $H_2O$  (Nitsch and Winkler, 1965; Holdaway, 1966). Taking into account the low Ps content in the relict clinzoisite, and inferring nearly isothermal conditions during the uplift (i.e.  $T \approx 600-650^\circ C$ ), the dehydration can develop at pressures  $\leq 0.4$  GPa (Boettcher, 1970). Low pressure conditions associated with the amphibolite facies overprint are consistent with the destabilisation of garnet, kyanite and staurolite in the host gneisses.

## ROCK CHEMISTRY

Analysed eclogites A (3) and B (6) show a common subalkalic basaltic composition in the TAS e Zr/TiO<sub>2</sub>-Nb/Y classificative diagrams (not reported). The high Fe/Mg (Mg# in the range 30.60-31.64 for Eclogites A; 27.44-34.37 for Eclogites B) and binary correlations (not reported) support strong fractionation along a tholeiitic trend.

Chondrite-normalised REE patterns (Fig. 6, Table 6)



have relatively flat trends about 10-30 times chondrite, with negative LREE fractionation ( $La_N/Sm_N = 0.44-1.03$  eclogites A;  $La_N/Sm_N = 0.52-0.57$  eclogites B) with the exception of sample D1 (eclogite A) showing relative enrichment of La, Ce and Nd ( $\Sigma LREE = 138$  ppm).

Type A eclogites show 1-3 MORB-normalised abundances (Fig. 7) with the exception of K, Ba and Rb. The occurrence of positive spikes in Ti, Zr, P with appreciable compositional variation from the same outcrop, and the scatter in most ternary and binary diagrams based on less mobile elements (Fig. 8), suggest an origin from Fe-Ti oxide enriched cumulates, consistent with the compositions observed in metabasites from the Migmatite Complex (Cappelli et al., 1992; Cruciani et al., 2001)

In such a context the high abundance of Ce, P, Nd in D1 can match localised apatite enrichment by cumulus. The high modal zircon in B1 cannot be ascribed to fractionation, taking into account the Mg#, Ti and P values. In analogy with the occurrences in Fe-Ti oxide gabbros from present-day ocean floors and in Jurassic Tethyan ophiolites, localised zircon enrichment can be ascribed to diorite veins in the basic protolith, homogenised during the metamorphic recrystallisation. Type B eclogites show relatively homogeneous composition, also with the amphibolites from the same unit (Oggiano and Di Pisa, 1992). On the whole, the REE and multivariation diagrams are consistent with evolved N-MORB liquids (Table 1). The N-MORB affinity results also from the element ratios (e.g.  $P_2O_5/Zr$ , Ti vs. Zr, Zr/Y vs. Zr and Ti/Y vs. Nb/Y, not reported) and in the La/10 - Y/15 - Nb/8 ternary diagram (Fig. 8).

Scattered values of Rb, Ba and K in both A and B types are likely due to mobilization.

Fig. 6 - REE patterns normalised according Nakamura (1974). Symbols as in Fig. 3. A: A-type eclogites. B: B-type eclogites.

Table 6 - Major, trace and RE element abundances of Type A and B eclogites.

Sample Eclogite Type <i>Tectonic complex</i>	A1 A <i>MC</i>	B1 A <i>MC</i>	D1 A <i>MC</i>	REC 3 B <i>GC</i>	REC 2 B <i>GC</i>	REC 3C B <i>GC</i>	REC 3BIS B <i>GC</i>	AV 27 B <i>GC</i>	AV35 B <i>GC</i>
Oxide wt%									
SiO <sub>2</sub>	48.30	48.80	47.20	46.60	45.80	46.00	46.50	50.60	47.70
TiO <sub>2</sub>	2.67	2.40	2.61	2.47	2.74	2.63	2.47	1.41	1.99
Al <sub>2</sub> O <sub>3</sub>	12.40	12.10	12.50	12.90	12.60	12.50	12.90	13.90	13.30
Cr <sub>2</sub> O <sub>3</sub>	0.02	0.02	0.02	0.00	0.01	0.02	0.00	0.01	0.02
Fe <sub>2</sub> O <sub>3</sub>	18.2	18.4	15.9	18.2	17.8	17.9	18.2	12.7	16.00
CaO	7.11	6.27	10.4	8.71	11.2	8.79	8.72	9.64	10.10
MgO	8.05	8.11	7.36	7.71	6.73	7.7	7.66	6.65	6.71
MnO	0.31	0.34	0.22	0.27	0.29	0.26	0.27	0.19	0.26
Na <sub>2</sub> O	1.93	1.81	2.47	2.09	2.23	2.12	2.08	2.54	2.36
K <sub>2</sub> O	0.23	0.23	0.08	0.12	0.04	0.13	0.12	0.87	0.17
P <sub>2</sub> O <sub>5</sub>	0.26	0.17	0.46	0.26	0.28	0.24	0.25	0.14	0.16
LOI	0.10	1.40	0.15	0.00	0.00	0.25	0.00	0.75	0.10
Sum	99.7	100.1	99.4	99.1	99.3	98.6	98.8	99.4	99.00
Trace ppm									
Ba	b.d.l.	46	b.d.l.	57	b.d.l.	21	55	72	27
Cr	128	119	119	111	121	120	b.d.l.	86	164
Nb	4	4	2	3	2	4	3	2	b.d.l.
Sr	99	80	163	112	91	116	112	181	59
Th	0.2	b.d.l.	0.5	0.5	0.3	0.3	0.3	0.3	0.2
U	0.1	0.1	0.2	b.d.l.	0.2	b.d.l.	0.1	b.d.l.	b.d.l.
Ni	49	48	38	41	60	47	b.d.l.	51	52
Rb	9	13	b.d.l.	3	5	b.d.l.	2	33	4
Y	44	31	47	48	49	51	48	30	39
Zr	163	259	149	144	130	145	142	76	92
REE ppm									
La	3.6	2.6	11.2	4.5	4.5	5.3	4.6	2.5	3.4
Ce	12.2	8.1	28.3	13.5	13.5	15.5	14.3	7	9.5
Pr	2.1	1.4	4.1	2.2	2.2	2.5	2.3	1.2	1.6
Nd	14.4	9.6	24.5	14.5	14.6	16	15.3	8.6	10.5
Sm	5	3.6	6.7	5.2	5.2	5.3	5.4	2.8	3.8
Eu	1.62	1.3	2.14	1.79	1.82	1.8	1.87	1.07	1.37
Gd	5.8	4.2	6.4	6	6.1	6.2	6.3	3.5	4.7
Tb	1.1	0.8	1.2	1.1	1.2	1.2	1.2	0.7	0.9
Dy	8.1	5.5	8.6	8.2	8.8	8.6	8.5	5.4	6.8
Ho	1.44	1	1.52	1.46	1.59	1.55	1.5	1	1.27
Er	5.7	3.9	6.2	5.7	6.2	6.2	5.9	3.9	4.9
Tm	0.9	0.6	1	0.9	0.9	1	1	0.6	0.8
Yb	5.1	3.7	5.7	5.3	5.6	5.8	5.5	3.6	4.6
Lu	0.6	0.44	0.66	0.61	0.66	0.67	0.62	0.42	0.52
La <sub>N</sub> /Yb <sub>N</sub>	0.57	0.54	0.61	0.49	0.46	0.56	1.31	0.47	0.47
La <sub>N</sub> /Sm <sub>N</sub>	0.53	0.53	0.62	0.55	0.55	0.52	1.03	0.44	0.44
Gd <sub>N</sub> /Yb <sub>N</sub>	0.90	0.87	0.85	0.81	0.77	0.91	0.89	0.91	0.91
ΣREE	288	298	310	233	180	300	365	195	276

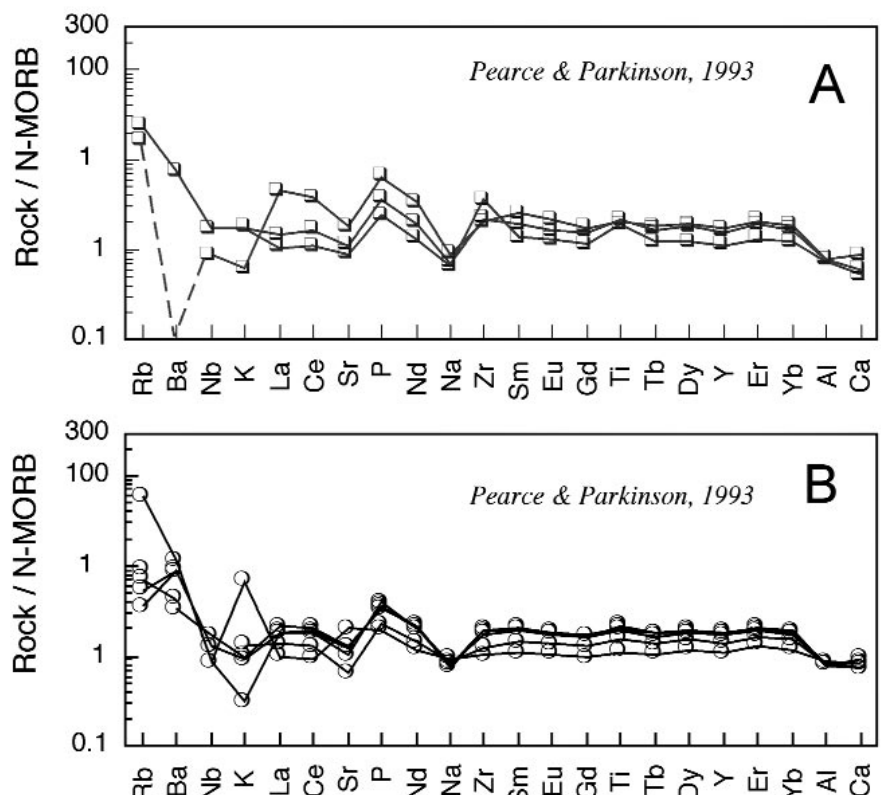


Fig. 7 - Rock / N-MORB ratio (normalization values after Pearce and Parkinson, 1993). Symbols as in Fig. 3. A: A-type eclogites. B: B-type eclogites.

## U/Pb RADIOMETRIC DATING

### Methods

Sample dissolution, chemical separation and mass spectrometry follow the techniques described in Paquette and Pin (2001). Total Pb blank were 4-10 pg for Pb and less than 1 pg for U during the analytical period. The U-Pb isotopic results were obtained on a Micromass VG Sector 54-30 mass spectrometer in a multicollector static mode;  $^{204}\text{Pb}$  was simultaneously measured with a Daly detector ion-counting system. Individual fraction ellipse errors ( $2\sigma$ ) and regression calculations were determined using the PbDat 1.24 and Isoplot/Ex 2.49 programs, respectively (Ludwig, 1993 and 2001). Age uncertainties are quoted at the  $2\sigma$  level. The decay constants used for the U-Pb system are those determined by Jaffrey et al. (1971) and recommended by the IUGS (Steiger and Jäger, 1977).

### Results

In sample ESC1C, two distinct zircon populations were separated. The first one comprises translucent, pinkish and prismatic crystals characterized by their elongation, thin oscillatory zoning and rounded edges (Plate 4D). These grains contain 18-20 ppm of radiogenic Pb (Table 7). Two multi-grains fractions were analyzed and plot on a concordant position defining an age at  $457 \pm 2$  Ma (Fig. 9). Considering the euhedral shape of the grains, this age is interpreted as a minimum estimate for the magmatism of the eclogite protolith. A small Pb-loss could have affected the zircons during the metamorphic event, slightly moving down the analytical points along the Concordia curve and possibly defining a younger age of 10-40 myr than the true magmatic emplacement. The second zircon population is made of rounded, very small, translucent and colourless grains containing 5-6 ppm of radiogenic Pb (Table 7). Cathodoluminescence im-

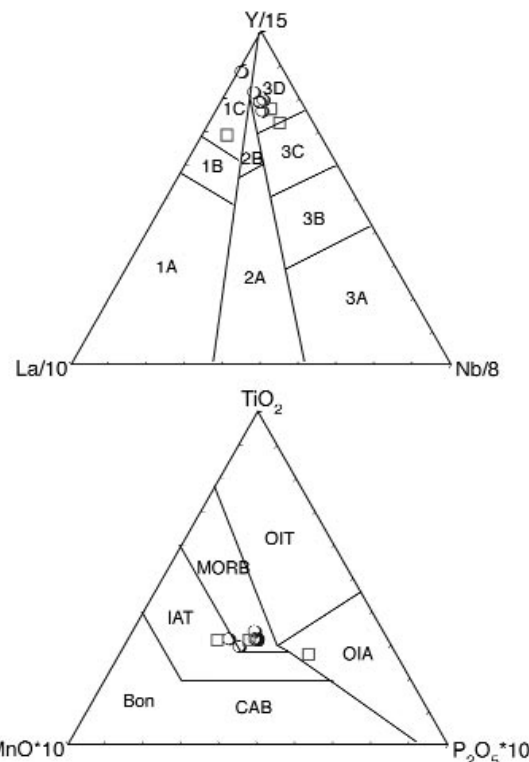


Fig. 8 - La/10 - Y/15 - Nb/8 ternary diagram (Cabans and Lecolle, 1989). Field 1C: volcanic arc tholeiites. Field 2B: back-arc basin. Field 3C: E-type MORB. Field 3D: N-type MORB. TiO<sub>2</sub>-P<sub>2</sub>O<sub>5</sub>\*10-MnO\*10: discrimination diagram for basalts after Mullen (1983).

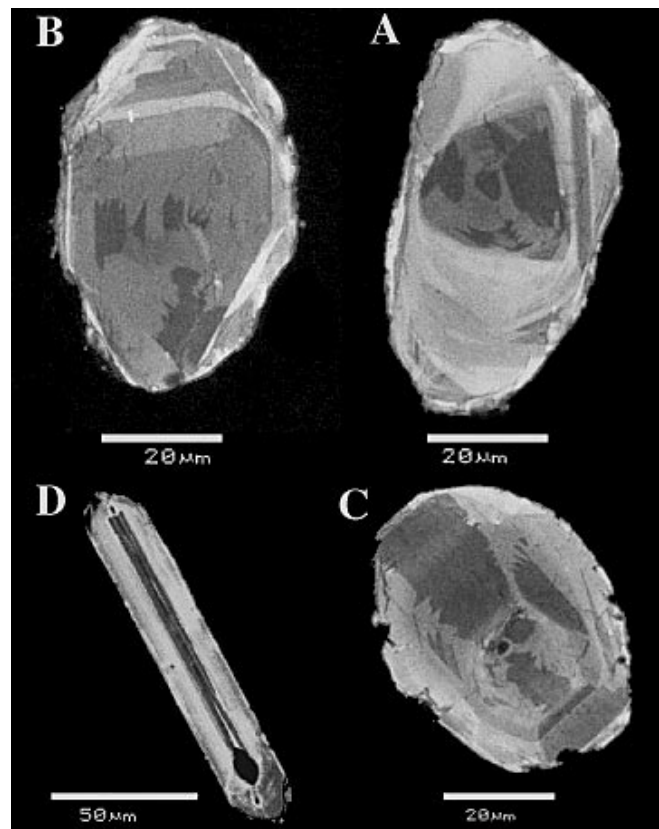


Plate 4 - Cathodoluminescence images of the analyzed zircons. A-C: rounded zircons with irregular and patchy zoning devoid of inherited cores. D: Euhedral elongated zircon with oscillatory zoning, rounded edges and possible thin inner channel.

ages show an irregular, chaotic and patchy zoning (Plate 4A-C) already observed in high-pressure zircons (Corfu et al., 2003). The two multi-grains analyzed fractions are concordant and define an age of  $403 \pm 4$  Ma (Fig. 9) interpreted as dating the zircon crystallization during the high-grade event. Finally, a fifth fraction, probably containing zircons from both populations, plot on intermediate location between the two intercepts. Such a feature is well known in U-Pb zircon dating of eclogites (Paquette et al., 1995).

### Regional comparisons

In the easternmost Migmatite Complex eclogites (Punta de Li Tulchi), U/Pb radiometric ages on zoned zircons yielded Upper Ordovician ages (450 Ma) assumed as protolith age, Siluro-Devonian ages ( $412 \pm 10$  Ma) inferred as eclogite peak, and  $\approx 330$  Ma ages considered as due to the Variscan metamorphic overprint (Palmeri et al., 1997).

Ages about 450 Ma in zircons from amphibolic migmatites have been referred to emplacement of the igneous protolith (Cruciani et al., 2001), consistent with the associated Tanaunella Orthogneisses ( $453 \pm 8$  Ma; Helbing, 2003).

Radiometric dating on the metabasites of the Gneiss Complex are so-far lacking, however, the Lodé Orthogneisses have been recognised as old as  $493 \pm 10$ , as the metarhyolites in the Ligurian Gneiss Amphibolite Complex (Helbing, 2003).

The amphibolite overprint affecting both the Migmatite and the Gneiss Complexes is referred to the Variscan collisional event and dated at  $315-320$  Ma (syn-S<sub>2</sub>, celadonite-poor white micas re-equilibrated during the D<sub>2</sub> stage; Di Vincenzo et al., 2003).

Table 7 - U/Pb data for ES1C sample.

n°	Fraction ( $\mu\text{m}$ )	Wt. (mg)	U (ppm)	Pb rad (ppm)	$^{206}\text{Pb}$ $^{204}\text{Pb}$	$^{208}\text{Pb}$ $^{206}\text{Pb}$	$^{206}\text{Pb}$ $^{238}\text{U}$	$^{207}\text{Pb}$ $^{235}\text{U}$	$^{207}\text{Pb}$ $^{206}\text{Pb}$	$^{206}\text{Pb}$ $^{238}\text{U}$	$^{207}\text{Pb}$ $^{235}\text{U}$	$^{207}\text{Pb}$ $^{206}\text{Pb}$	correl. coeff.	
<i>atomic ratios</i>														
<i>apparent ages</i>														
1	[5] euh. pi.	0,019	213	18,0	1166	0,2805	0,0736 ± 4	0,571 ± 6	0,0563 ± 5	458	459	464	0,59	
2	[5] euh. pi.	0,009	251	19,8	801	0,2188	0,0729 ± 8	0,566 ± 11	0,0563 ± 9	454	455	465	0,59	
3	[7] rnd. cl.	0,042	81	5,6	3290	0,0808	0,0710 ± 2	0,547 ± 3	0,0559 ± 3	442	443	447	0,61	
4	[10] rnd. cl.	0,022	91	5,8	733	0,1210	0,0645 ± 8	0,491 ± 11	0,0552 ± 10	403	406	422	0,58	
5	[10] rnd. cl.	0,010	102	6,8	547	0,2139	0,0644 ± 12	0,490 ± 18	0,0552 ± 16	402	405	421	0,58	

Individual analyses were performed on the least magnetic ( $2^\circ$  forward and side tilt at 2.2 A using a Frantz Isodynamic magnetic barrier separator) crack-free zircon grains. The isotopic ratios are corrected for mass discrimination ( $0.1 \pm 0.015\%$  per amu for Pb and U), isotopic tracer contribution and analytical blanks: 4-10 pg for Pb and less than 1 pg for U. Initial common Pb is determined for each fraction in using the Stacey and Kramers (1975) two-step model. Absolute errors corresponding to the last significant digits are given at the 2s level. Number in brackets is number of grains in fraction. Abbreviations: rad = radiogenic ; euh. = euhedral; rnd. = rounded; cl. = colourless; pi. = light pink.

## DISCUSSION AND GEODYNAMIC INFERRENCES

The high-grade metamorphic Variscides of Sardinia consist of: I) a metamorphic migmatite complex, where metabasites locally preserving eclogite relict are associated with orthogneissic lenses. The metabasites preserve trace of igneous fractionation, and have a whole MORB to transitional tholeiitic signature. II) A medium-grade metapelite - quartzite complex with metabasites that only locally show eclogite relicts. An origin from N-MOR basalts is suggested.

In the Migmatite Complex metabasites record a high P/high T event followed by nearly isothermal uplift towards metamorphic conditions intermediate between high-T amphibolite and granulite facies conditions. The temperatures and the thermal gradients attained by eclogites and the temperatures and thermal gradients during the exhumation are likely higher than in the Gneiss Complex.

In both complexes, gradients exceeding  $10^\circ\text{C/km}$ , and likely  $\geq 15^\circ\text{C/km}$  are reliably inferred. In particular, in the Migmatite Complex higher thermal gradients ( $\geq 25^\circ\text{C/km}$ ) occurred during the uplift, further increased

Although in the Migmatite Complex the differential rheology in eclogites and host migmatites erased textural relationships, the occurrence of relict kyanite in migmatites and the consistent thermobaric evolution between metabasites and migmatites support a common origin within a subducted slab formed by sedimentary protoliths associated with acidic and basic, mostly subvolcanic, bodies.

The metamorphic path of the Migmatite Complex, points to a quasi – isothermal uplift. Structural evidence suggests that the granulite event occurred in a still active collisional setting. The uplift of the metamorphic complex coincides with the switch from an underplating-kinematics characterised by transport normal to the collision, to an oblique kinematics with transport parallel to the belt (Carosi and Oggiano, 2002). Conversely, the latest low P anatetic event (about 300 Ma in age) broadly coeval with the emplacement of the Sardinia Batholith and with vertical shortening should be referred to the post-collisional collapse of the belt.

In most metabasites of the Gneiss Complex, relicts of the eclogite event are lacking; more data are needed to choose between the following: I) amphibolites originate from complete re-equilibration of eclogites or II) amphibolites represent prograde steps of the evolution within the subducted slab that produced the eclogites. In this hypothesis, metabasites sampled at different depths were involved in the same tectonic units during their uplift and underwent low pressure amphibolite facies to low grade retrograde evolution.

The retrograde, low P, amphibolite facies overprint in the Gneiss Complex is referred to the collisional stage of the Variscan orogen. Only at few sites, the post-collision HT / LP overprint affects the complex (Asinara Island, Coghinas Lake), giving rise to widespread And+Crds±Sil association. Furthermore, partial melting did not occur in this unit.

Striking similarities arise with the pre-Namurian basement of the Ligurian Alps (Desmons et al., 1999; Cortesogno

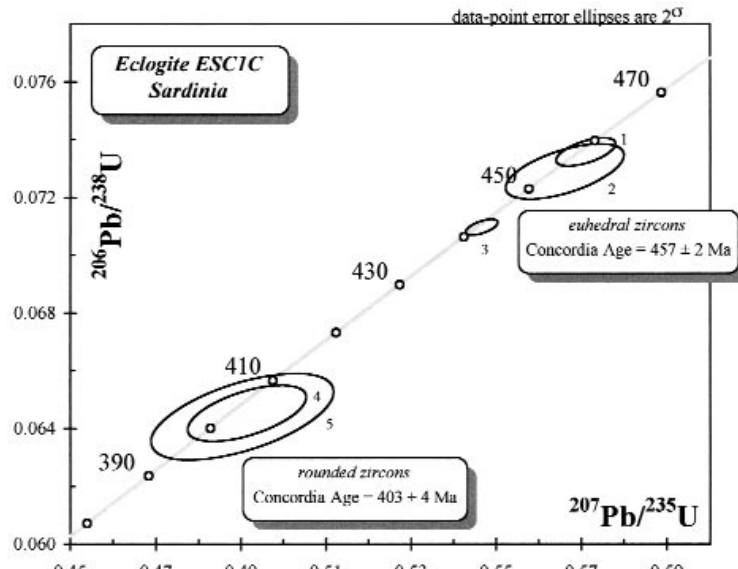


Fig. 9 - Concordia diagram for ES1C, A-type eclogite.

no et al., 1993; Gaggero et al., 2004), where two different eclogite-bearing complexes occur:

I) Eclogites within stromatitic and nebulitic migmatites (Migmatite-Eclogite Complex) have tholeiitic compositions, and likely originated from intrusive fractionated protoliths (Cortesogno et al., 1997). The biotite-, sillimanite- garnet-rich paleosome of migmatites suggests a pelite protolith.

The metamorphic peak attaining T about 760°C for minimum P  $\approx$  1.7 GPa (omphacite-garnet and garnet-phengite pairs) was followed by exhumation through granulite facies conditions. The granulite facies is characterised by scant orthopyroxene occurrence in clinopyroxene, garnet, hornblende, plagioclase ( $An_{35}$ ) assemblages. A gabbroic intrusion in migmatites includes cm to m-sized nodules of eclogite relicts. In Al-rich nodules, phlogopite and kyanite relicts are replaced by sillimanite-, corundum-, sapphirine-, ilmenite-, hercynite-bearing assemblages. High T, low P conditions in migmatites are evidenced by localised andalusite blasts. Radiometric data are lacking.

II) Rare metabasite bodies preserving garnet and symplectite textural relicts, associated with quartzites and kyanite+staurolite+garnet-bearing paragneisses, occur within a Gneiss – Amphibolite complex, affected by polyphase pre-Alpine metamorphism and represented by kyanite+sillimanite+staurolite+garnet paragneisses, diopside- or garnet-bearing amphibolites and orthogneisses. The paragneisses originate from arkosic protoliths; quartzites, micaschists and rare hornblende marbles are interlayered, commonly surrounding the metabasites. The metabasites, originated from MORB-type protoliths, are locally interbedded and likely coeval with acidic metavolcanites dated at the Early Ordovician (~500 Ma). Minor serpentinised ultrabasic bodies also occur within the gneissic sequence. The age of the earlier metamorphic event is considered as lying between two granitoid intrusions dated at about 490 and 480 Ma respectively.

Both the Migmatite-Eclogite and the Gneiss-Amphibolite Complexes, involved in Variscan megafold structures, were overprinted by medium P amphibolite facies metamorphism at 327 Ma (Del Moro et al., 1982).

Despite the large incompleteness of radiometric dating it seems reasonable to correlate the Ligurian Gneiss-Amphibolite Complex with the Sardinia Gneiss Complex and the Migmatite-Eclogite Complex with the Migmatite Complex respectively, on the base of petrologic convergence and also taking into account the vicinity of Sardinia and Ligurian Alps at Upper Carboniferous-Lower Permian times.

If so, the Gneiss-Amphibolite and Gneiss Complexes represent an older history beginning during a Neoproterozoic (?) Cambro-Ordovician rifting (bimodal tholeiitic basalts and rhyolite volcanism) within a quartzite-pelite-arenite sedimentary sequence attaining incipient oceanisation (mantle ultramafics) later subducted and intruded by granite melts during the Early - Middle Ordovician. The Ligurian Migmatite-Eclogite and the Sardinia Migmatite Complexes originated from Upper Ordovician tholeiitic intrusives (and ultramafites?) associated with a pelitic-arenitic sequence together with coeval acidic igneous rocks in an extensional context. The Siluro-Devonian subduction was followed by (rapid) uplift under high T regime; finally during the Carboniferous, both the subducted belts were involved in the lowermost high-grade levels of the Variscan nappe pile.

Metabasites preserving eclogite relicts occur in most segments of the Variscan belt throughout Europe, from Spain to the Bohemian massif, The tholeiitic (e.g. Bodinier et al., 1981) to alkalic (e.g. von Raumer et al., 1990) compositions,

the local association with ultramafites and the Neo-Proterozoic, Upper Cambrian and Lower Ordovician protolith ages are consistent with a geodynamic Cambro-Ordovician extensional setting, sometimes attaining oceanisation, followed by collision and subduction. Estimated ages of the eclogite peak mostly range from Middle – Late Ordovician to Siluro-Devonian. Carboniferous ages at about 316-358 Ma are reported for high pressure metabasites and peridotites from the South Carpathian pre-Alpine nappe (Medaris et al., 2003). Therefore, diachronous collisional events are stressed out.

The occurrence of different P-T conditions of the eclogite metamorphism in sequences overprinted by Variscan amphibolite facies conditions in Saxonian Erzgebirge has been assumed as evidence of different nappe Units (Schmädicke et al., 1992; Mingram, 1998; Rötzler et al., 1998).

In many segments of the Variscan belt, the PT conditions evaluated for the eclogite event and the exhumation paths suggest that the lithospheric isotherms were relatively shallow along some collision fronts (Eastern Alps: Frisch et al., 1990; Sassi et al., 1987; Matte, 1991; eastern Austrides, Calabria: Miller and Thöni, 1997; Fornelli et al., 2002; Grassner and Schenk, 2001; external massifs of the Western Alps, Paquette et al., 1985); however, low T conditions for Devonian subduction are reported for the Ile de Groix area (Shelley and Bossière, 2000; Schultz et al., 2001; Ballèvre et al., 2003) and West Sudetes in the Bohemian Massif (Patočka et al., 1996). Moreover, ultra-high pressure settings along low thermal gradients (5-10°C/km) are indicated, for the Saxonian Erzgebirge (Schmädicke et al., 1991).

The paleoenvironmental restorations of the extensional basins evidence differing geodynamic environments from crustal thinning and rifting to oceanised crust. Thus, correlations between the nature of the subducted slab, depth of subduction and the developed gradients can be envisaged.

The diachronous subductions and accretions among microplates during the collision of the Laurussia and Hun superterrane (von Raumer et al., 2003) during the suture of the aborted Rheic basin, were followed by nappe stacking and fast exhumation during the Late Carboniferous and by subsequent Westphalian to lower Permian orogenic collapse, associated with transtensional tectonics.

## ANALYTICAL METHODS

Major elements in the mineral phases were analyzed at Genoa University using a Philips SEM 515 scanning electron microscope equipped with an EDAX PV9100 spectrometer in the energy-dispersive mode. Operating conditions were 15 kV accelerating voltage and 2.1 nA of beam current. Na<sub>2</sub>O and MgO contents analyzed in silicates by means of an EDAX microprobe are generally underestimated if the analysis is processed with current automatic methods. To overcome this problem, the background value for Na (1.040 keV) and Mg (1.252 keV) was manually corrected and considered to be between 0.9 and 4.2 keV.

Atomic proportions of pyroxene were calculated assuming stoichiometry and charge balance. Nomenclature follows the scheme of Morimoto et al. (1988), amplified by Rock (1990) for Na-Ca and Na-pyroxenes. The Ca-amphiboles cation sum was normalised to 13-(Ca+Na+K), as suggested by Laird and Albee (1981); Fe<sup>3+</sup> = 46-total cation charge and Fe<sup>2+</sup> = Fe<sub>tot</sub>-Fe<sup>3+</sup>; Al<sup>IV</sup> = 8-Si, Al<sup>VI</sup> = Al<sub>tot</sub>-Al<sup>IV</sup>. Leake et al. (1997)'s nomenclature was adopted. Plagioclase was normalised to 5 cations and 8 oxygens. Garnet was recast to 5 cations and 12

oxygens. Epidote was normalised to 12.5 oxygens. Abbreviations for minerals are according to Kretz (1983).

Whole-rock major and trace element abundances for the metabasites were carried out by XRF techniques at the X-RAL Laboratories Canada. Losses on ignition (LOI) were determined by the gravimetric method. RE elements were analysed by ICP-MS at the X-RAL Laboratories, Canada.

## ACKNOWLEDGEMENTS

This research was made possible by MIUR - COFIN 2001 funds to L. Cortesogno and G. Oggiano. The authors thank the constructive revision of J. von Raumer (Fribourg, CH) and B. Lombardo (Turin, I).

## REFERENCES

- Ai Y., 1994. A revision of the garnet-clinopyroxene  $\text{Fe}^{2+}$ - $\text{Mg}^{2+}$  exchange thermometer. *Contrib. Miner. Petrol.*, 115: 467-473.
- Ballèvre M., Pitra P. and Bohn M., 2003. Lawsonite growth in the epidote blueschists from the Ile de Groix (Armorican Massif, France): a potential geobarometer. *J. Met. Geol.*, 21 (7): 723-735.
- Barca S., Durand Delga M., Rossi P. and Storch P., 1996. The Pan-African micaschists of Corsica (France) and their Palaeozoic cover: Their place in the Variscan orogen of Southern Europe. *C.R. Acad. Sci. Ser. II*, 322 (11): 981-989.
- Blundy J.D. and Holland T.J.B., 1990. Calcic amphibole equilibria and a new amphibole-plagioclase geothermometer. *Contrib. Miner. Petrol.*, 104: 208-224.
- Bodinier J.L., Giraud A., Dupuy C., Leyreloup A., and Dostal J., 1981. Caractérisation géochimique des metabasites associées à la suture méridionale hercynienne: Massif Central français et Chamrousse (Alpes). *Bull. Soc. Géol. France*, 2: 115-124.
- Boettcher A.L., 1970. The system  $\text{CaO-Al}_2\text{O}_3-\text{SiO}_2-\text{H}_2\text{O}$  at high pressures and high temperatures. *J. Petrol.*, 11 : 337-379.
- Cabanis B. and Lecolle M., 1989. Le diagramme La/10 - Y/15 - Nb/8: un outil pour la discrimination des séries volcaniques et la mise en évidence des processus de mélange et/ou de contamination crustale. *C.R. Acad. Sci. Ser. II*, 309: 2023-2029.
- Cappelli B., Carmignani L., Castorina F., Di Pisa A., Oggiano G. and Petrini R., 1992. A Hercynian suture zone in Sardinia: geological and geochemical evidence. *Geodin. Acta*, 7: 31-43.
- Carmignani L. and Oggiano G., 1997. Terranes in the Variscan segment of Sardinia: a tentative approach. In: IGCP PROJECT N°276 "Terrane maps and terrane description" *Ann. Géol. Pays Hellén.*, 37: 199-209.
- Carmignani L., Carosi R., Di Pisa A., Gattiglio M., Musumeci G., Oggiano G. and Pertusati P.C., 1994. The Hercynian chain in Sardinia (Italy). *Geodin. Acta*, 7 (1): 31-47.
- Carosi R. and Palmeri R., 2002. Orogen - parallel tectonic transport in the Variscan belt of north-eastern Sardinia (Italy): implications for the exhumation of medium-pressure metamorphic rocks. *Geol. Mag.*, 139: 95-102.
- Carosi R. and Oggiano G., 2002. Transpressional deformation in northwestern Sardinia (Italy): insights on the tectonic evolution of the Variscan belt. *Comptes Rendus Geosci.*, 334: 287-294.
- Carpenter M.A., 1980. Mechanism of exsolution in sodic pyroxenes. *Contrib. Mineral. Petrol.*, 71: 289-300.
- Corfu F., Hanchar J.M., Hoskin P.W.O. and Kinny P., 2003. Atlas of zircon textures. In: J.M. Hanchar and P.W.O. Hoskin (Eds), *Zircon. Mineral. Soc. Am.*, 53: 568-600.
- Cortesogno L., Dallagiovanna G., Gaggero L. and Vanossi M., 1993. Elements for the Palaeozoic history of the Ligurian Alps. In: J. Von Raumer and D. Neubauer (Eds.), *Pre-Alpine geology*. Springer Verlag, p. 257-277.
- Cortesogno L., Gaggero L. and Capelli C., 1997. Petrology of pre-Alpine eclogites and amphibolites from the Ligurian Briançonnais basement. *Atti Ticinensi. Sci. Terra*, 39: 3-29.
- Cortesogno L., Gaggero L. and Oggiano G., 2000. Different tectono-thermal evolution in eclogitic rocks from the axial zone of Sardinia Variscan chain. In: *Variscan - Appalachian dynamics: the building of the Upper Palaeozoic basement, 15th Basement Tectonic, A Coruna, Spain, Abstract vol.*: p.212.
- Cruciani G., Franceschelli M., Caredda A.M. and Carcangiu G., 2001. Anatexis in the Hercynian basement of NE Sardinia, Italy: a case study of the migmatite of Porto Ottiolu. *Mineral. Petrol.*, 71: 195-233.
- Dahl P.S., 1980. The thermal-compositional dependence of  $\text{Fe}^{2+}$ - $\text{Mg}^{2+}$  distribution between coexisting garnet and pyroxene: applications to geothermometry. *Am. Mineral.*, 65: 852-866.
- Del Moro A., Di Pisa A., Oggiano G. and Villa I.M., 1991. Isotopic ages of two contrasting tectono-metamorphic episodes in the Variscan chain in northern Sardinia. *Geologia del Basamento Italiano*, Siena 21-22 marzo 1991. Abstract Volume.
- Del Moro A., Pardini G., Messiga B. and Poggio M., 1982. Dati petrologici e radiometrici preliminari sui massicci cristallini della Liguria occidentale. *Rend. S. I. M. P.*, 38 (1): 73-87.
- Desmons J., Compagnoni R., Cortesogno L., Frey M. and Gaggero L., 1999. Pre-Alpine metamorphism of the Internal zones of the Western Alps. *Schweiz. Miner. Petr. Mitt.*, 79: 23-39.
- Di Pisa A., Gattiglio M. and Oggiano G., 1992. Pre-Hercynian magmatic activity in the nappe zone (internal and external) of Sardinia: evidence of two within-plate basaltic cycles. *IGCP N. 276, Newsletter*, 5: 107-116.
- Di Vincenzo G., Carosi R. and Palmeri R., 2004. The relationship between tectono-metamorphic evolution and argon isotope records in white mica: constraints from *in situ*  $^{40}\text{Ar}$ - $^{39}\text{Ar}$  laser analysis of the Variscan basement of Sardinia (Italy). *J. Petrol.*, 45: 1013-1043.
- Ellis D.J. and Green, D.H., 1979. An experimental study of the effect of Ca upon garnet-clinopyroxene Fe-Mg exchange equilibria. *Contrib. Mineral. Petrol.*, 71: 13-22.
- Elter F.M., 1987. La fascia blastomylonitica tardo ercinica della Valle del Posada nella zona assiale della Sardegna. PhD Thesis, Univ. Siena, 122 pp.
- Essene E.J. and Fyfe W.S., 1967. Omphacite in Californian metamorphic rocks. *Contrib. Mineral. Petrol.*, 15: 1-23.
- Evans B.W. and Ghiorso M.S., 1995. Thermodynamics and petrology of cummingtonite. *Am. Mineral.*, 80: 649-663.
- Fornelli A., Piccarreta G., Del Moro A. and Acquafrredda P., 2002. Multi-stage melting in the lower crust of the Serre (southern Italy). *J. Petrol.*, 43: 2191-2217.
- Franceschelli M., Carcangiu G., Caredda A.M., Cruciani G., Memmi I. and Zucca M., 2002. Transformation of cumulate mafic rocks to granulite and re-equilibration in amphibolite and greenschist facies in NE Sardinia, Italy. *Lithos*, 63: 1-18.
- Franceschelli M., Eltrudis A., Memmi I., Palmeri R. and Carcangiu G., 1998. Multistage metamorphic re-equilibration in eclogitic rocks from the Hercynian basement of NE Sardinia (Italy). *Mineral. Petrol.*, 62: 167-193.
- Frisch W., Ménöt R.P., Neubauer F. and von Raumer J.F., 1990. Correlation and evolution of the Alpine basement. *Schweiz. Miner. Petrogr. Mitt.*, 70: 265-285.
- Gaggero L., Cortesogno L. and Bertrand J.M., 2004. The Pre-Namurian Basement of the Ligurian Alps: a review of the lithostratigraphy, pre-Alpine metamorphic evolution, and regional comparisons. *Per. Min.*, 73, Spec. Iss., 2: 85-96.
- Ganguly J., 1979. Garnet and clinopyroxene solid solution and geothermometry based on Fe-Mg distribution coefficient. *Geochim. Cosmoch. Acta*, 43: 1021-1029.
- Ghezzo C., Memmi I. and Ricci C.A., 1979. Un evento granulitico nel basamento metamorfico della Sardegna nord-orientale. *Mem. Soc. Geol. It.*, 20: 23-38.
- Ghezzo C., Memmi I. and Ricci C.A., 1982. Le eclogiti e le granuliti della Sardegna nord-orientale. In: L. Carmignani, T. Cozzola, C. Ghezzo, P.C. Pertusati, C.A. Ricci (Eds), *Guida alla geologia del Paleozoico Sardo. Guide Geol. Regionali. Soc. Geol. It.*, p. 151-156.
- Ghiorso M.S., Evans B.W., Hirschmann M.M. and Yang H. 1995. Thermodynamics of the amphiboles: Fe-Mg cummingtonite

- solid solutions. *Amer. Mineral.*, 80: 502-519.
- Grässner T. and Schenk V., 2001. An exposed Hercynian deep crustal section in the Sila Massif of Northern Calabria: mineral chemistry, petrology and a P-T path of granulite-facies metapelitic migmatites and metabasites. *J. Petrol.*, 42: 931-961.
- Holdaway M.J., 1966. Hydrothermal stability of clinozoisite plus quartz. *Am. J. Sci.*, 264: 643-667.
- Holland T. and Blundy J., 1994. Non-ideal interactions in calcic amphiboles and their bearing on amphibole-plagioclase thermometry. *Contrib. Mineral. Petrol.*, 116: 433-447.
- Holland T.J.B., 1983. The experimental determination of activities in disordered and short-range ordered jadeitic pyroxenes. *Contrib. Mineral. Petrol.*, 82: 214-220.
- Jaffrey A.H., Flynn K.F., Glendenin L.E., Bentley W.C., Essling A.M., 1971. Precision measurement of half-lives and specific activities of  $^{235}\text{U}$  and  $^{238}\text{U}$ . *Phys. Rev.*, C4: 1889-1906.
- Kretz R., 1983. Symbols for rock-forming minerals, *Am. Miner.* al., 68: 277-279.
- Krogh E.J., 1988. The garnet-clinopyroxene Fe-Mg geothermometer-a reinterpretation of coexisting experimental data. *Contrib. Mineral Petrol.*, 66: 75-80.
- Laird J. and Albee A.L., 1981. Pressure, temperature, and time indicators in mafic schists: their application to reconstructing the polymetamorphic history of Vermont. *Am. J. Sci.*, 281: 127-175.
- Leake B.E., Wolley A.R., Arps C.E.S., Birch W.D., Gilbert M.C., Grice J.D., Hawthorne F.C., Kato A., Kish H., Krivovichev V.G., Linthout K., Laird J., Mandarino J.A., Maresch W.V., Nickel E.H., Rock N.M.S., Schumacher J.C., Stephenson N.C.N., Ungaretti L., Whittaker E.J.W. and Youzhi G., 1997. Nomenclature of amphibole: report of the subcommittee on amphiboles of the International Mineralogical Association, Commission on new minerals and mineral names. *Canad. Mineral.*, 35: 219-246.
- Ludwig K.R., 1993. Pbdat: a computer program fro processing Pb-U-Th isotope data, version 1.24. US Geol. Survey, Open-File Rep., 88-542, 32 pp.
- Ludwig K.R., 2001. User manual for Isoplot/Ex rev. 2.49. A geochronological toolkit for Microsoft Excel. Berkeley Geochron. Center Spec. Publ., 1a, 56 pp.
- Matte Ph., 1991. Accretionary history and crustal evolution of the Variscan belt. *Tectonophysics*, 196: 309-337.
- Medaris G. Jr., Ducea M., Ghent E and, Iancu V., 2003. Conditions and timing of high pressure Variscan metamorphism in the South Carpathian, Romania. *Lithos*, 70: 141-161.
- Miller C., Sassi F.P. and Armari G. 1976. On the occurrence of altered eclogitic rocks in north-eastern Sardinia and their implications. *N. Jb. Paläont. Mh.*, 11: 683-689.
- Miller Ch. and Thöni M., 1997. Eo-Alpine eclogitisation of Permian MORB-type gabbros in the Koralpe (Eastern Alps, Austria): new geochronological, geochemical and petrological data. *Chem. Geol. (Isotope Geosci. Section)*, 137: 283-310.
- Mingram B., 1988. The Erzebirge a subducted part of Northern Gondwana: Geochemical evidence for repetition of early Palaeozoic metasedimentary sequences in metamorphic thrust units. *Geol. Mag.*, 135: 785-801.
- Morimoto N., Fabries J., Ferguson A.K., Ginzburg I.V., Ross M., Seifert F.A., Zussman J., Aoki K. and Gottardi G., 1988. Nomenclature of pyroxenes. *Am. Mineral.*, 73: 1123-1133.
- Mullen E.D., 1983.  $\text{MnO}/\text{TiO}_2/\text{P}_2\text{O}_5$ ; a minor element discriminant for basaltic rocks of oceanic environments and its implications for petrogenesis. *Earth Planet. Sci Lett.*, 62: 53-62.
- Nakamura N., 1974. Determination of REE, BA, Fe, Mg, Na and K in carbonaceous and ordinary chondrites. *Geochim. Cosmochim. Acta*, 38: 757-775.
- Nitsch K.H. and Winkler H.G.F., 1965. Bildungsbedingung von Epidot und Orthozoisit. *Beitr. Min. Petr.*, 11: 470-486.
- Oggiano G. and Di Pisa A., 1992. Geologia della catena ercina in Sardegna-Zona Assiale. In: *Struttura della Catena Ercinica in Sardegna (Gruppo informale di Geologia strutturale, Eds)*, 147-177.
- Palmeri R., Fanning M., Franceschelli M., Memmi I and Ricci C.A., 1997. New petrological and geochronological data on the eclogite of P.ta de li Tulchi, NE Sardinia (Italy). 5<sup>th</sup> Int. Eclogite Conf., Terra Nova, 9, Abstr. Suppl., 1: 24.
- Paquette J.L. and Pin C., 2001. A new miniaturized extraction chromatography method for precise U-Pb zircon geochronology. *Chem. Geol.*, 176: 311-319.
- Paquette J.L., Ménot R.P. and Peucat J.J., 1985. Sm-Nd and U-Pb zircon study of eclogites from the Alpine external massifs (Western Alps): evidence for crustal contamination. *Earth Plan. Sci. Lett.*, 96: 181-198.
- Paquette J.L., Monchoux P. and Couturier M. 1995. Geochemical and isotopic study of a norite-eclogite transition in the European Variscan belt: implications for U-Pb zircon systematics in metabasic rocks. *Geochim. Cosmochim. Acta*, 59 (8): 1611-1622.
- Patocka F., Pivec E. and Oliveriova D., 1996. Mineralogy and petrology of mafic blueschists from the Rychory Mts crystalline complex (West Sudetes, Bohemian Massif). *N. Jahr. Mineral. Abh.*, 170 (3): 313-330.
- Pattison D.R.M. and Newton R.C., 1989. Reversed experimental calibration of the garnet-clinopyroxene Fe-Mg exchange thermometer. *Contrib. Miner. Petrol.*, 101: 87-103.
- Pearce J.A. Parkinson I.J., 1993. Trace element models for mantle melting: application to volcanic arc petrogenesis. In: Prochard, Alabaster, Harris, Neary eds. 1993 *Magmatic processes and plate tectonics*, Geol. Soc. London Spec. Publ., 76, 373-403.
- Powell R., 1985. Regression diagnostics and robust regression in geothermometer/geobarometer calibration: the garnet-clinopyroxene geothermometer revisited. *J. Metam. Geol.*, 3: 231-243.
- Rock N.M.S., 1990. The International Mineralogical Association (IMA/CNMMN) Pyroxene Nomenclature Scheme: Computerization and its consequences. *Mineral. Petrogr.*, 43: 211-227.
- Rötzler K., Schumacher R., Maresch W. and Willner A.P., 1998. Characterization and geodynamic implication of contrasting metamorphic evolution in juxtaposed high pressure units at the Western Erzebirge (Saxony, Germany). *Eur. J. Mineral.*, 10: 261-280.
- Sassi F.P., Zanferrari G. and Zirpoli G., 1987. The Caledonian event in the Eastern Alps: a review. In: *Pre-Variscan and Variscan events in the Alpine-Mediterranean mountain belts*. Alpha, Bratislava, p. 431-434.
- Schmädicke E., Okrusch M. and Schmidt W., 1992. Eclogite-facies rocks in the Saxonian Erzebirge, Germany: high-pressure metamorphism under contrasting P-T condition. *Contrib. Miner. Petrol.*, 110: 226-241.
- Schulz B., Triboulet C., Audren C., Pfeifer H.R. and Gilg A., 2001. Two-stage prograde and retrograde Variscan metamorphism of glaucophane-eclogites, blueschists and greenschists from Ile de Groix (Brittany, France). *Int. J. Earth Sci.*, 90 (4): 871-889.
- Shelley D. and Bossière G., 2000. A new model for the Hercynian Orogen of Gondwanan France and Iberia., *J. Struct. Geol.*, 22 (6): 757-776.
- Solar G.S. and Brown M., 2001. Petrogenesis of migmatites in Maine, USA. Possible source of peraluminous granite in plutons. *J. Petrol.*, 42: 789-823.
- Stacey J.S. and Kramers J.D., 1975. Approximation of terrestrial lead isotope evolution by a two-stage model. *Earth Planet. Sci. Lett.*, 26: 207-221.
- Stampfli G.M., von Raumer J.F. and Borel G.D., 2002. The Paleozoic evolution of pre-Variscan terranes: from Gondwana to the Variscan collision. *Geol. Soc. Am. Spec. Paper*, 364: 263-280.
- Steiger R.H. and Jäger E., 1977. Subcommission on geochronology: convention to use of decay constants in geo and cosmochronology. *Earth Planet Sci Lett.*, 26: 207-221.
- von Raumer J.F., Galetti G., Pfeiffer H.R. and Oberhansli R. 1990. Amphibolites from Lake Emosson / Aiguilles Rouges, Switzerland: tholeiitic basalts of a Paleozoic continental rift zone. *Schweiz. Mineral. Petrogr. Mitt.*, 70: 419-435.
- von Raumer J.F., Stampfli G.M. and Bussy F., 2003. Gondwana-derived microcontinents - the constituents of the Variscan and Alpine collisional orogens. *Tectonophysics*, 365 : 7-22.

Received, March 9, 2004

Accepted, September 20, 2004